iScience

CellPress
OPEN ACCESS

Article

eys$^{+/-}$; *lrp5*$^{+/-}$ Zebrafish Reveals Lrp5 Can Be the Receptor of Retinol in the Visual Cycle

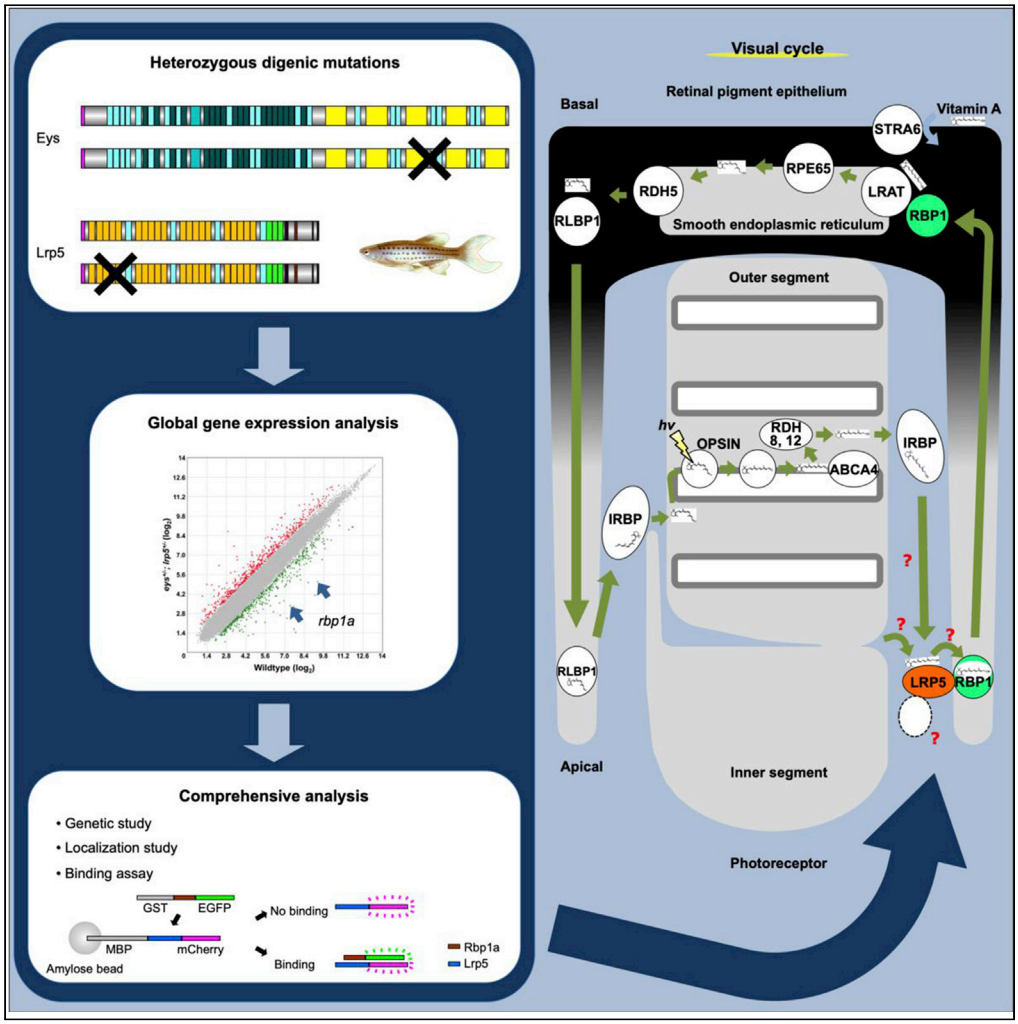

Shimpei Takita, Yuko Seko

ShimpeiTakita_papers@hotmail.com (S.T.)
seko-yuko@rehab.go.jp (Y.S.)

HIGHLIGHTS

eys$^{+/-}$; *lrp5*$^{+/-}$ zebrafish showed mild photoreceptor degeneration

Microarray analysis identified dramatical decrease of *rbp1a* expression

Rbp1a protein was colocalized with Lrp5 protein at the microvilli of the RPE

Rbp1a directly bound to the C-terminal intracellular region of Lrp5 *in vitro*

Takita & Seko, iScience *23*, 101762
December 18, 2020
https://doi.org/10.1016/j.isci.2020.101762

iScience

CellPress
OPEN ACCESS

Article

eys$^{+/-}$; *lrp5*$^{+/-}$ Zebrafish Reveals Lrp5 Can Be the Receptor of Retinol in the Visual Cycle

Shimpei Takita[1,*] and Yuko Seko[1,2,*]

SUMMARY

Vision is essential for vertebrates including humans. Sustained vision is accomplished by retinoid metabolism, the "visual cycle," where all-*trans* retinol (atROL) is incorporated into the retinal pigment epithelium (RPE) from photoreceptors presumably through decade-long missing receptor(s). Here, we show that the LDL-related receptor-5 (Lrp5) protein is linked to the retinol binding protein 1a (Rbp1a), the transporter of atROL in the visual cycle, by generating and analyzing the digenic *eyes shut homolog*$^{+/-}$; *lrp5*$^{+/-}$ zebrafish, the same form of gene defect detected in a human case of inherited retinal degeneration. Global gene expression analysis followed by genetic study clarified that *rbp1a* played a role downstream of *lrp5*. Rbp1a protein was colocalized with Lrp5 protein at microvilli of RPE cells. Furthermore, Rbp1a directly bound to the C-terminal intracellular region of Lrp5 *in vitro*. Collectively, these results strongly suggest that Lrp5 is a potent candidate of the receptor of atROL in the visual cycle.

INTRODUCTION

In the vertebrate retina, two types of photoreceptors mainly mediate vision: rods and cones (Kawamura and Tachibanaki, 2008). Upon light absorption by the visual opsins, their chromophore, 11-*cis* retinal, is converted to all-*trans* retinol (atROL) and is released from rods and cones. Sustained vision, essential for vertebrates including humans, is accomplished by retinoid metabolism, the "visual cycle" (Lamb, 2013; Sparrow et al., 2010), where atROL is incorporated into the adjacent retinal pigment epithelium (RPE), isomerized to the 11-*cis* isomer, and transported back to photoreceptors. The uptake of atROL by RPE cells is thought to be mediated by a membrane receptor (Sparrow et al., 2010); however, the entity has been unknown for a decade.

Human *eyes shut homolog* (*EYS*) gene (Online Mendelian Inheritance in Man no. 612424), a homolog of the *Drosophila* eyes shut/spacemaker (*eys*) (Abd El-Aziz et al., 2008; Collin et al., 2008), is a major causative gene of nonsyndromic autosomal recessive retinitis pigmentosa (RP) (Abd El-Aziz et al., 2008; Hosono et al., 2012; Iwanami et al., 2012), and later analyses using next-generation sequencing (NGS) extended that mutations in *EYS* also cause cone-rod dystrophy (CRD) (Katagiri et al., 2014; Pierrache et al., 2019). RP, the most common genetic disorder among the inherited retinal dystrophies, is characterized by progressive visual loss caused by degenerative abnormalities of rods, and CRD is initiated by degenerative abnormalities of cones. Therefore, human genomics suggests that EYS protein function(s) crucially contribute to both rods and cones.

Previous studies using zebrafish ortholog si:ch211-69e5.1 or *eys* from our and other laboratories indicate that the full-length Eys protein may be important for Eys protein function(s) in terms of its pathogenesis (Lu et al., 2017; Takita et al., 2019) and that dysfunction of ciliary pocket of cones observed in *eye*$^{-/-}$ zebrafish may be the cause of photoreceptor degeneration (Yu et al., 2016); however, exact molecular function of Eys in photoreceptors is still not well understood.

Recently, a possibility emerged from a human case report in a Chinese family by a targeted NGS approach that digenic heterozygous form of mutations in the *low-density lipoprotein* (*LDL*)*-related receptor-5* (*LRP5*) and *EYS* genes (*EYS*$^{+/-}$; *LRP5*$^{+/-}$) might cause RP (Gao et al., 2017). LRP5 protein, a member of the LDL receptor superfamily, is best known as a co-receptor for Wnt ligands involved in the wingless (Wnt) signaling pathway on cell membranes, which is essential for the development of vascular endothelial cells, Müller cells, and retinal interneurons (Tamai et al., 2000). LRP5 is also reported to be involved in cholesterol

[1]Visual Functions Section, Department of Rehabilitation for Sensory Functions, Research Institute, National Rehabilitation Center for Persons with Disabilities, 4-1 Namiki, Tokorozawa, Saitama 359-8555, Japan

[2]Lead Contact

*Correspondence: ShimpeiTakita_papers@hotmail.com (S.T.), seko-yuko@rehab.go.jp (Y.S.)

https://doi.org/10.1016/j.isci.2020.101762

and glucose uptake (Chin et al., 2015; Fujino et al., 2003), and its possible involvement in vitamin A (i.e., atROL) system cells is also suggested (Figueroa et al., 2000).

LRP5 is known to cause familial exudative vitreoretinopathy (FEVR) (Gong et al., 2001; Li et al., 2018; Yang et al., 2012); however, the form of the mutation in *LRP5* found in the pedigrees of FEVR is typically autosomal recessive (Li et al., 2018; Yang et al., 2012) and no mutations have been linked to RP so far (https://sph.uth.edu/retnet/). Mutations causing RP in *EYS* are also believed to be typically recessive (Iwanami et al., 2012). Therefore, it was necessary to examine the possible pathogenesis of the digenic $EYS^{+/-}$; $LRP5^{+/-}$ mutations, apparently a rare form of mutation, using animal models carrying the same form of mutations. More importantly, because the digenic mutations in *peripherin* (*PRPH2*) and *ROM1* cause RP and they physically interact with each other (Goldberg and Molday, 1996; Kajiwara et al., 1994), we presumed that it would not be unreasonable to also assume a similar scenario, that EYS and LRP5 proteins may interact with each other and the reduced expression levels of normal EYS and LRP5 proteins may not be sufficient enough to sustain the maintenance of photoreceptor function in patients, which may cause RP. If this hypothesis is correct, it could help elucidate the molecular function(s) of EYS and/or LRP5 proteins.

Here, we show that the digenic $eys^{+/-}$; $lrp5^{+/-}$ heterozygous mutations cause mild photoreceptor degeneration. Global gene expression analysis of the $eys^{+/-}$; $lrp5^{+/-}$ eye by the microarray reveals the remarkable decrease in the expression level of the *retinol binding protein 1a* (*rbp1a*) gene, which encodes the transporter of atROL in the RPE in the visual cycle (Lamb, 2013; Sparrow et al., 2010), and therefore it appears to be the hallmark of the digenic mutations. We further show that Lrp5 protein is a strong candidate for the receptor of atROL being involved in the uptake of atROL with Rbp1a in the RPE in the visual cycle.

RESULTS

Digenic $eys^{+/-}$; $lrp5^{+/-}$ Zebrafish Shows Signs of Mild Photoreceptor Degeneration

In the previous human case report (Gao et al., 2017), the possibility that $EYS^{+/-}$; $LRP5^{+/-}$ might cause RP is reported based on single male patient from single family. To examine whether the digenic heterozygous mutations would lead photoreceptor degeneration under experimental conditions, we first generated zebrafish mutants carrying digenic $eys^{+/-}$; $lrp5^{+/-}$ mutations by crossing the $eys^{sa31957}$ ($eys^{+/-}$) and $lrp5^{sa11097}$ ($lrp5^{+/-}$) mutant lines (Figure 1A, arrows; Figures S1A and S1B; obtained from the Zebrafish International Resource Center [ZIRC]) as a complementary genetic study using tractable animal models. At 14 months post fertilization (mpf), we sectioned the eyes and measured the thickness of the photoreceptor cell layer (PRCL) and number of nuclei in the outer nuclear layers (ONL). The thickness of the PRCL and the number of nuclei in the ONL of the $eys^{+/-}$; $lrp5^{+/-}$ mutants were 10% and 16% reduced compared with that of wild-type PRCL or ONL, respectively (Figure 1B, middle and right panels, respectively). The result showed mild photoreceptor degeneration in the digenic $eys^{+/-}$; $lrp5^{+/-}$ mutant retina. In addition, thickness of the RPE layer was 14% thinner in the $eys^{+/-}$; $lrp5^{+/-}$ eye than in the wild-type eye (Figure S2A). No reduction in the thickness of PRCL or number of nuclei in the ONL was observed in the single $eys^{+/-}$ or $lrp5^{+/-}$ mutant eye (Figures S2B and S2C). Therefore, retinal changes were not due to either of the single mutations, but rather due to the digenic mutations.

We also performed TUNEL staining using 8 mpf eye sections to examine apoptosis in the PRCLs (Figure S3). In wild-type adult eyes, we detected almost no apoptotic cells in all of the cell layers in the retina or retinal pigment epithelium (RPE) (Figure S3A). In contrast, in the digenic $eys^{+/-}$; $lrp5^{+/-}$ mutant eyes (Figure S3C), apoptotic cells were sparse but were detected in the central region of PRCL, RPE cell layer, retinal ganglion cell layer, and inner nuclear layer. In the peripheral regions, apoptosis was intensely observed in all of the cell layers. These results also support the hypothesis that $EYS^{+/-}$; $LRP5^{+/-}$ cause RP in humans, which was proposed in the previous study (Gao et al., 2017).

Identification of *rbp1a* as a Remarkably Downregulated Gene in the $eys^{+/-}$; $lrp5^{+/-}$ Mutant Eyes

In previous studies in the $eys^{-/-}$ zebrafish, apoptosis is observed at 6, 8, and 14 mpf and the ratio of apoptosis increases with age (Lu et al., 2017; Yu et al., 2016). Also, the expression levels of marker proteins appear normal at least until 2 mpf. Therefore, we performed microarray analysis at 3.5 mpf so as to capture such candidate genes that would show remarkable decrease in the expression levels, caused more directly by the dysfunction of the genes in the initial phase rather than other genes in which marked decrease in the

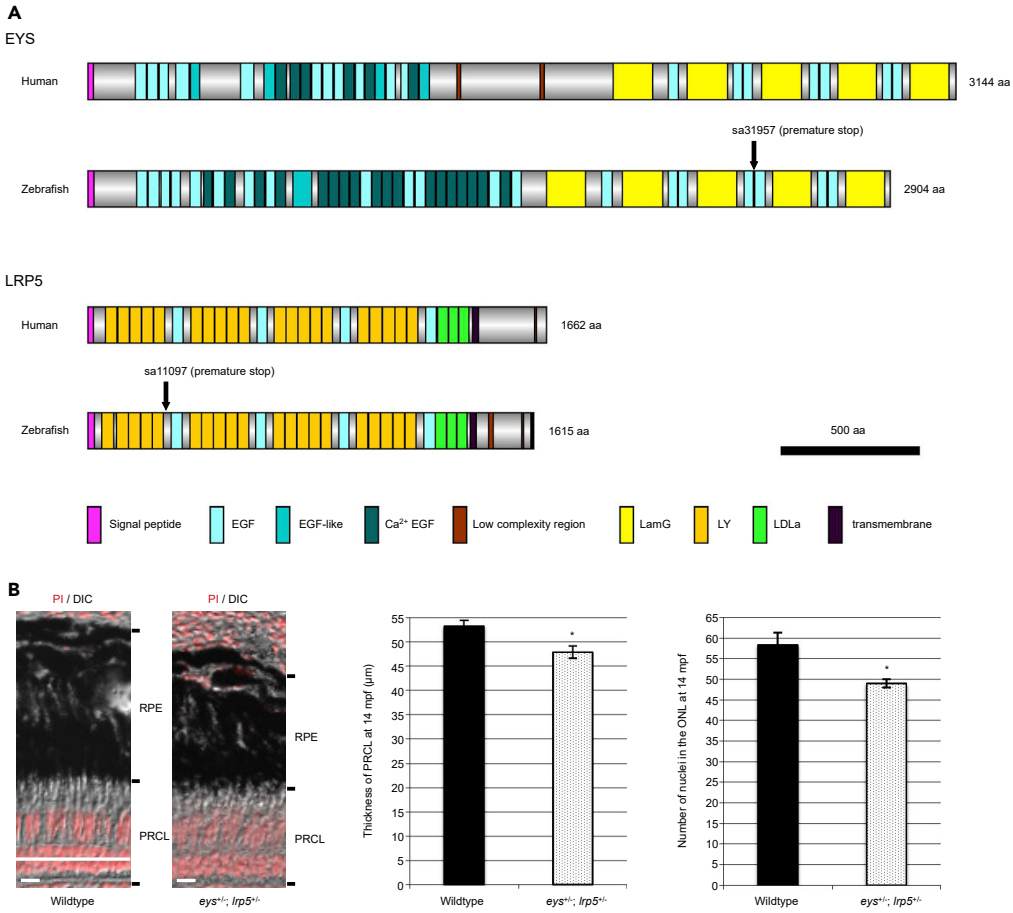

Figure 1. Conservation of Human and Zebrafish EYS and LRP5 Proteins and Mild Photoreceptor Degeneration in the Digenic *eys*$^{+/-}$; *lrp5*$^{+/-}$ Zebrafish

(A) The domain structures of human and zebrafish EYS and LRP5 proteins show that the compositions of EYS and LRP5 proteins are well conserved between the two species. Human and zebrafish EYS proteins consist of a signal peptide sequence for secretion, epidermal growth factor (EGF), EGF-like and Ca^{2+} EGF domains in the N-terminal half, and laminin A G-like (LamG) and EGF domains in the C-terminal half. Human and zebrafish LRP5 proteins consist of a signal peptide sequence, low-density lipoprotein receptor YWTD (LY; also known as β-propeller), EGF, and LDLa domains in the N-terminal extracellular half followed by transmembrane region and low complexity region in the C-terminal intracellular region. Vertical arrows in zebrafish EYS and LRP5 proteins indicate the point mutations resulting in premature stop codons (nonsense mutations).

(B) The thickness of photoreceptor cell layer (PRCL) was 10% reduced in the *eys*$^{+/-}$; *lrp5*$^{+/-}$ zebrafish eyes compared with wild-type PRCL at 14 mpf (wild-type, 53.3 ± 1.1 μm; *eys*$^{+/-}$; *lrp5*$^{+/-}$ mutants, 47.9 ± 1.2 μm). The number of nuclei in the ONL was reduced 16% in the *eys*$^{+/-}$; *lrp5*$^{+/-}$ zebrafish eyes compared with wild-type PRCL (wild-type, 58.3 ± 3.1; *eys*$^{+/-}$; *lrp5*$^{+/-}$ mutants, 49 ± 1.0). Data are represented as mean ± SD. *p < 0.01. DIC, differential interference contrast; mpf, months post fertilization; RPE, retinal pigment epithelium. Scale bars, 10 μm.

expression levels can be attributed to the secondary effect caused by the increased apoptosis in PRCL and other layers in the retina, which could mask crucial genes essential for photoreceptors.

In the *eys*$^{+/-}$; *lrp5*$^{+/-}$ eyes, 0.89% (529 genes) of total genes (59,384) were upregulated and 0.80% (473 genes) were downregulated (Figures 2A–2C). Among the genes, *mhc2a1* was the one that was most down-regulated (Figure 2D, fold change, 0.0159). *mhc2a1* is one of the major histocompatibility complex (MHC) class II genes that are known to be critical for the cellular immune response (Bander et al., 1997) and are related to apoptotic pathways; the main function is to present processed antigens (Holling et al., 2004). Therefore, it appeared that the decrease in the expression level of *mhc2a1* was more related to cell survival in response to the abnormality in the digenic *eys*$^{+/-}$; *lrp5*$^{+/-}$ heterozygous mutations than was related to specific Eys and/or Lrp5 function(s).

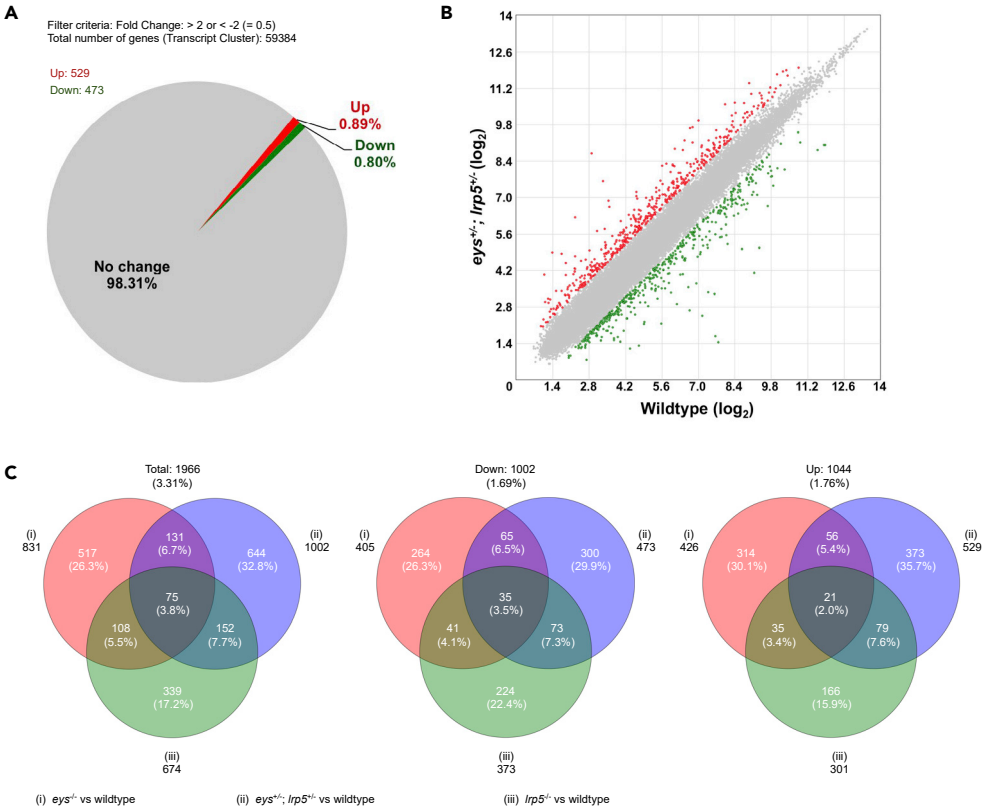

D

ID	Signal for *eys*$^{+/-}$; *lrp5*$^{+/-}$ (log_2)	Signal for wildtype (log_2)	Fold change	Gene symbol; Accession
13282534	1.67	7.65	0.0159	mhc2a1; NM_131695
13293908	4.11	9.14	0.0305	?
13304984	5.08	9.33	0.0524	si:ch211-119o8.7 (*rbp1a*)
13083422	3.37	7.38	0.0620	si:ch211-119o8.7 (*rbp1a*)
13124388	2.67	6.66	0.0627	GENSCAN00000008112
13302386	5.03	8.68	0.0798	?
13184368	2.16	5.57	0.0943	LOC103911364
12991151	1.31	4.72	0.0943	ubald1a?
13125972	2.90	6.18	0.1033	LOC100006764
13301580	3.71	6.91	0.1083	?
13303716	1.20	4.37	0.1110	?
13008466	3.56	6.61	0..1110	rlim?
13303714	6.68	9.66	0.1266	aga
13304056	6.68	9.66	0.1266	aga
13204872	5.22	8.12	0.1332	?

Figure 2. Global Gene Expression Analysis of the Digenic *eys*$^{+/-}$; *lrp5*$^{+/-}$ Zebrafish Eyes Identifies the *retinol binding protein 1a* (*rbp1a*) Gene.

(A and B) About 1.69% (1,002 genes) were 2-fold changed among the 59,384 transcript clusters (genes) in the *eys*$^{+/-}$; *lrp5*$^{+/-}$ zebrafish eyes compared with the eyes of wild-type siblings (A). About 0.80% (473 genes) of the total were 2-fold downregulated and 0.89% (529 genes) were 2-fold upregulated (B, green and red spots, respectively).

(C) About 3.31% (1,966 genes) were 2-fold changed, 1.69% (1,002) genes were 2-fold downregulated, and 1.76% (1,044 genes) were 2-fold upregulated in the *eys*$^{-/-}$, *lrp5*$^{-/-}$, or *eys*$^{+/-}$; *lrp5*$^{+/-}$ eyes compared with the eyes of wild-type siblings (left, middle, and right panels, respectively). Among 0.80% (473 genes) 2-fold downregulated in the *eys*$^{+/-}$; *lrp5*$^{+/-}$ eyes (middle panel), 21.1% (100 genes) were overlapped with the eyes of *eys*$^{-/-}$ siblings and 14.6% (108 genes) were overlapped with the eyes of *lrp5*$^{-/-}$ siblings.

(D) Genes whose expression levels were dramatically changed were extracted. "Fold change" in the fourth column indicates the ratio (the bare value of the signal for *eys*$^{+/-}$; *lrp5*$^{+/-}$ divided by that for the wild-type). The ratio for si:ch211-119o8.7 (the *rbp1a* gene, third and fourth rows) was identified as the gene remarkably downregulated in the *eys*$^{+/-}$; *lrp5*$^{+/-}$ eyes (fold changes, 0.0524 (ID: 13304984) and 0.0620 (13083422)). "Signal for *eys*$^{+/-}$; *lrp5*$^{+/-}$" (second column) and "Signal for wild type" (third column) are shown in (log_2).

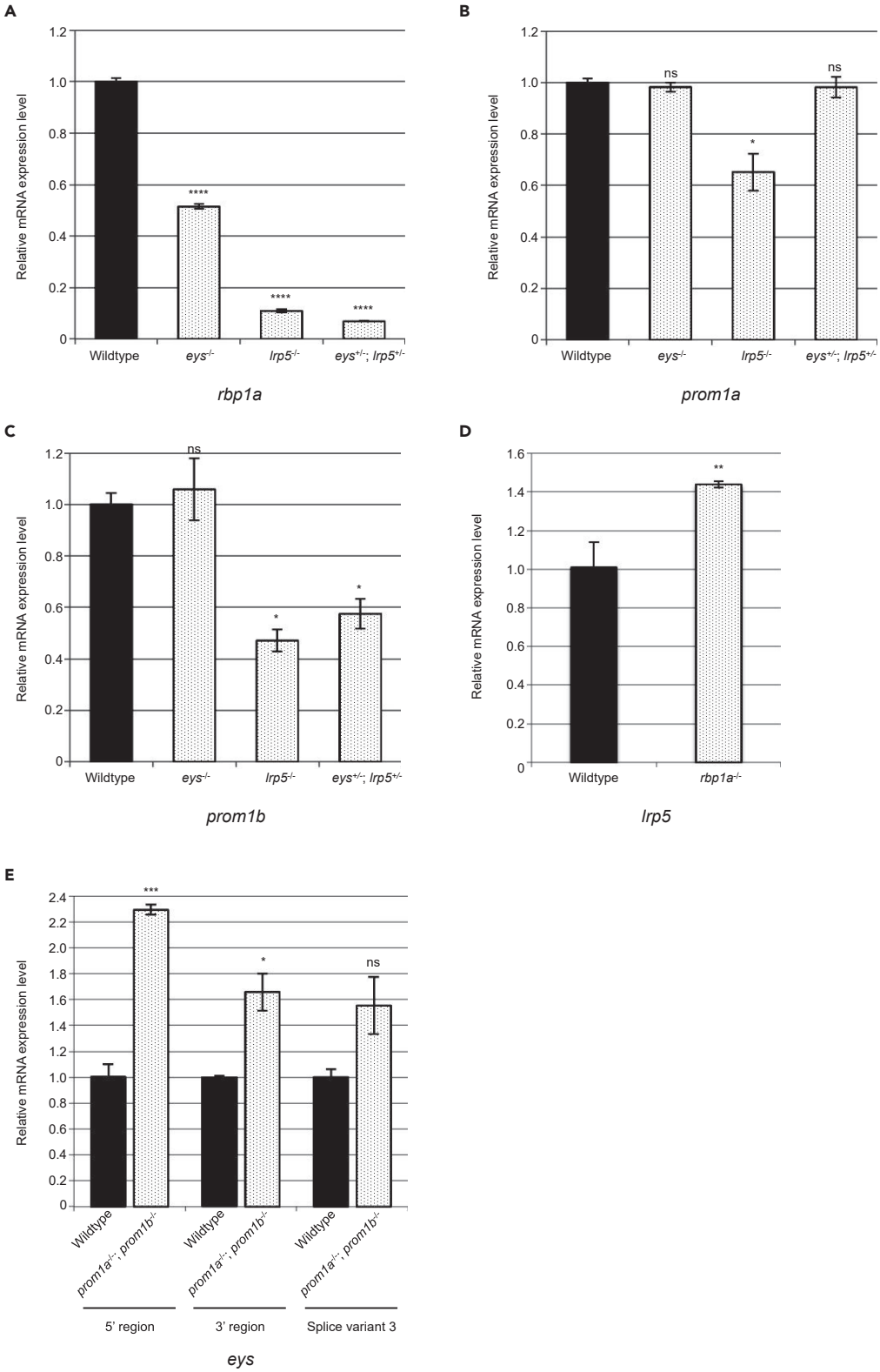

Figure 3. The *rbp1a* Gene Plays a Role Downstream of the *lrp5* Gene

(A) qPCR analysis showed that the expression level of the *rbp1a* gene was remarkably decreased in the $lrp5^{-/-}$ (~11%) and digenic $eys^{+/-}$; $lrp5^{+/-}$ (~7%) eyes while moderately decreased in the $eys^{-/-}$ eyes (~51%) compared with wild-type eyes at 3.5 mpf.

Figure 3. *Continued*

(B and C) There was no change in the expression level of either the *prom1a* or *prom1b* gene in the $eys^{-/-}$ eyes compared with wild-type eyes at 3.5 mpf.

(D) The expression level of the *lrp5* gene was not remarkably changed in the $rbp1a^{-/-}$ eyes (~142%) compared with wild-type eyes at 3.5 mpf. The *rbp1a* gene played a role downstream of the *lrp5* gene (A and D).

(E) The expression level of the *eys* gene was slightly increased in the $prom1a^{-/-}$; $prom1b^{-/-}$ eyes (~229% for 5′ region, ~166% for 3′ region, and ~155% for splice variant 3 [Takita et al., 2019]) compared with wild-type eyes at 3.5 mpf. Negative genetic interaction between the *eys* gene and the *prom1a* or *prom1b* gene was not observed (B, C, and E).

All data are represented as mean ± SD. *p < 0.005, **p < 0.0005, ***p < 0.0001, ****p < 0.000001. Ns, not significant.

The gene that was second-most downregulated in the digenic eyes compared with wild-type siblings was si:ch211-119o8.7 (*rbp1a*, *rbp1.2*) (Figure 2D, fold changes, 0.0524 and 0.0620). RBP1 protein (i.e., CRBP) is well known to be involved in the transport of atROL in the RPE in the visual cycle (Lamb, 2013; Sparrow et al., 2010). In addition, $Rbp1^{-/-}$ mice are shown to cause photoreceptor outer segment degeneration under vitamin A-deficient diet conditions (Ghyselinck et al., 1999). Furthermore, in zebrafish, there is a paralog, *rbp1b* (*rbp1.1*). The expression level of *rbp1b* determined by cap analysis of gene expression (CAGE) (Takita et al., 2019) is 12.8% of that of *rbp1a*, indicating that *rbp1a* is the predominant gene expressed in the eye (Figure S2D). Also, the expression level of *rbp1b* was also 20% reduced in the digenic eye (Figure S2E). These lines of evidence convinced us to pursue the *rbp1a* gene as the most relevant among the candidates for the related genes in the initial phase.

We then confirmed the downregulation of *rbp1a* by quantitative real-time PCR (qPCR). The expression levels of *rbp1a* in the $eys^{+/-}$; $lrp5^{+/-}$, $eys^{-/-}$, and $lrp5^{-/-}$ mutant eyes were 6.8%, 51.4%, 10.9% compared with wild-type eyes, respectively (Figure 3A). Besides, no change was observed in the expression level of *prom1a* or *prom1b* (Figures 3B and 3C, respectively). The qPCR results were in good agreement with the microarray results.

We also checked the expression levels of Rbp1a protein with immunohistochemistry at 8 mpf (Figure S4). Rbp1a was immunopositive for particle-shaped structures (spots) in which RBP1a was concentrated at the microvilli of the RPE (see next subsection for the detailed localization analysis). At 8 mpf, in the $eys^{+/-}$; $lrp5^{+/-}$ mutant adult eyes, the signal intensity of Rbp1a was decreased, which was consistent with the mRNA expression, immunopositive spots were more sporadic, and each spot was wider compared with the ones in wild-type eyes (Figures S4C and 4A, respectively). Therefore, *rbp1a* appeared to be the most probable candidate for the cause of RP in the human case report and we decided to focus on *rbp1a* in more detail.

Colocalization of Lrp5 and Rbp1a Proteins in the Outer Retina

Because the Rbp1 protein is known to play an important role in the visual cycle (Lamb, 2013; Sparrow et al., 2010), we next sought to determine how the remarkable downregulation of the gene might be related to the Eys and/or Lrp5 proteins. First, we raised an antibody against zebrafish Rbp1a protein and examined its localization in the adult eye by immunohistochemistry. Immunopositive signal for Rbp1a was observed in the outer retina (Figures 4A, S5A, and S5B). As Rbp1a is known to be localized to the microvilli in the RPE (Bonilha et al., 2004; Huang et al., 2009), eyes were next co-stained with the antibody to MOESIN (MSN) (Figure 4B), one of three closely related ERM (EZRIN, RADIXIN, MSN) proteins (Berryman et al., 1993) and a marker for the microvilli of the RPE (Bonilha et al., 2004). Staining of Rbp1a overlapped well with that of MSN (Figure 4C, arrowheads) with one exception that the most concentrated regions were MSN negative. In contrast, co-staining with anti-Lrp5 antibody (Figures 4C and 4D) revealed that Lrp5 protein colocalized with Rbp1a protein at the most concentrated regions in the microvilli of the RPE (Figure 4D, arrowheads), which was very close to the inner segment of photoreceptors in the outer retina.

We also stained the eye with anti-fibrillary acidic protein (GFAP) and anti-glutamine synthetase (GS) to visualize the processes of Müller cells. The upper-most intensities of the signal were observed in the lower part of ONL where nuclei of rods and UV cones are located (Figures S5E and S5F). Co-stained with the antibody to Rbp1a also clarified that the upper signals were located within the microvilli of RPE cells, whereas the lower signals were located within the processes of Müller cells (Figure S5G, arrows and arrowheads, respectively).

Direct Binding of Rbp1a Protein and C-Terminal Intracellular Region of Lrp5 Protein *In Vitro*

The colocalization of **Lrp5** and **Rbp1a** proteins suggests that they may form a complex at the microvilli of the RPE, indicative of possible involvement of Lrp5 in the uptake of atROL. In order to test the possibility

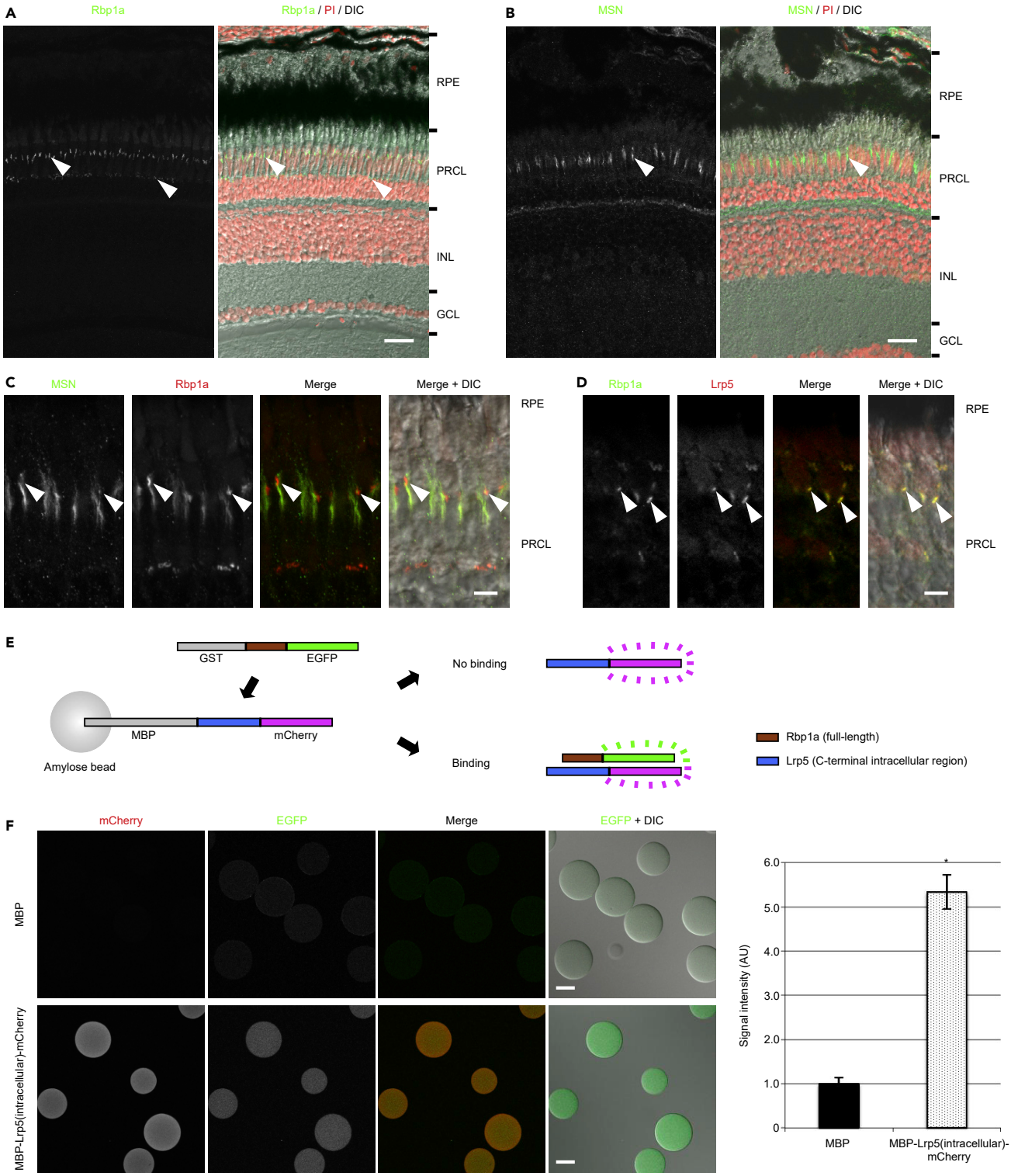

Figure 4. Lrp5 and Rbp1a Proteins Are Colocalized in the Outer Retinas and Bind Directly *In Vitro*.

(A) Staining of Rbp1a protein was observed in the outer retina (arrowheads). Nuclei were stained with propidium iodide (PI) (red).

(B and C) Rbp1a signal overlapped well with MOESIN (MSN), a marker of the microvilli of the RPE, and strong signal was observed at the tip (arrowheads), which suggested that Rbp1a was concentrated in the tip of the microvilli in the RPE.

Figure 4. *Continued*

(D) Staining of Lrp5 protein with Rbp1a protein revealed that Lrp5 was colocalized with Rbp1a at the concentrated region (tip) of the microvilli of the RPE (arrowheads).

(E) Experimental design of binding assay. Binding is detected by fluorescence from EGFP.

(F) EGFP signal was observed on the beads in which the intracellular region of Lrp5 protein was fused to MBP (lower panels), whereas it was not detected on the beads in which MBP alone was present (upper panels) (MBP, 1.0 ± 0.1 for 8 beads; MBP-Lrp5(intracellular)-mCherry, 5.3 ± 0.4 for 6 beads).

Data are represented as mean ± SD. *p < 0.0000005. DIC, differential interference contrast; GCL, ganglion cell layer; INL, inner nuclear layer; PRCL, photoreceptor cell layer; RPE, retinal pigment epithelium. Scale bars, 20 μm in (A) and (B), 5 μm in (C) and (D), and 50 μm in (F).

more rigorously *in vitro*, the direct binding of RBP1a and C-terminal intracellular region of Lrp5 was examined using purified N-terminally GST-fused and C-terminally EGFP-fused RBP1a (GST- RBP1a -EGFP) and either MBP or N-terminally MBP-fused and C-terminally mCherry-fused C-terminal intracellular region of Lrp5 (MBP- Lrp5 (intracellular)-mCherry) pre-bound to amylose beads (Figure 4E), which is under the concept of binding assay similar to Agrin and Lrp4 (Kim et al., 2008; Zhang et al., 2011). Although EGFP signal was not observed with MBP alone (Figure 4F, upper panels), the signal was observed with Lrp5-fused MBP (MBP- Lrp5 (intracellular)-mCherry) (Figure 4F, lower panels). These results show the direct binding of Rbp1a to the C-terminal intracellular region of Lrp5 *in vitro*.

The *rbp1a* Gene Plays a Role Downstream of the *lrp5* Gene in the Eye

The expression level of the *rbp1a* gene was remarkably decreased (~10%) compared with the wild-type siblings in the $lrp5^{-/-}$ adult eyes (Figure 3A). To examine the possibility that the *rbp1a* and *lrp5* genes could interact with each other in the eye, $rbp1a^{-/-}$ zebrafish was generated by the CRISPR-Cas9 system (Figure S1C) and the expression level of the *lrp5* gene in the $rbp1a^{-/-}$ eyes was measured by qPCR at 3.5 mpf. The qPCR analysis showed that the expression level of *lrp5* was not remarkably changed in the $rbp1a^{-/-}$ adult eyes compared with the wild-type siblings (~142%) (Figure 3D). The genetic study clarified that $rbp1a^{-/-}$ played a role downstream of *lrp5* rather than genetically interacting with each other.

DISCUSSION

In the present study, we showed photoreceptor degeneration and remarkably decreased expression level of the *rbp1a* gene in the digenic $eys^{+/-}$; $lrp5^{+/-}$ zebrafish. Localization studies revealed that the Rbp1a protein is colocalized with the Lrp5 protein at the microvilli of the RPE. We showed the direct binding of Rbp1a to the C-terminal intracellular region of Lrp5 *in vitro*. Our genetic analysis clarified the role that *rbp1a* plays downstream of *lrp5*. These results strongly suggest that Lrp5 and Rbp1a proteins form a complex at the microvilli of the RPE and that Lrp5 may be involved in the uptake of atROL in the visual cycle.

Photoreceptor Degeneration and Implication for Possible Treatment for Digenic $eys^{+/-}$; $lrp5^{+/-}$ Mutations

In this study, we showed in zebrafish that the thickness of the PRCL in the $eys^{+/-}$; $lrp5^{+/-}$ mutants is mildly reduced compared with that of the wild-type PRCL. The results using the zebrafish model strongly support the previous human genomic analysis that $EYS^{+/-}$; $LRP5^{+/-}$ might cause RP, which is based on one patient from a single family. In addition, because the RPE layer was thinner and apoptosis was also observed in the RPE layer, the RPE was degenerating as well as the photoreceptors in the $eys^{+/-}$; $lrp5^{+/-}$ mutants.

We next showed by global gene expression analysis that the expression level of *rbp1a* is remarkably decreased in the $eys^{+/-}$; $lrp5^{+/-}$ mutant eye. Rbp1 protein is involved in the transport of atROL in the RPE in the visual cycle. Furthermore, in mice, knockout of the ortholog, *Rbp1*, causes photoreceptor outer segment abnormalities under vitamin A-deficient diet conditions (Ghyselinck et al., 1999). Therefore, vitamin A ingestion may help prevent or slow the progression of photoreceptor degeneration in the digenic $eys^{+/-}$; $lrp5^{+/-}$ heterozygous mutations in humans.

Lrp5 Is a Strong Candidate for the Receptor of atROL

It has not been clear whether the uptake of atROL on the apical surface of the RPE in the visual cycle is mediated by a protein docking or receptor-mediated protein interaction(s) (Cook et al., 2017). On the basal side of the RPE, uptake of atROL is mediated by "stimulated by retinoic acid gene 6" (STRA6), the receptor for retinol binding protein (Kawaguchi et al., 2007). Accordingly, STRA6 is reported not to be expressed on the apical surface of the RPE (Kawaguchi et al., 2007); however, some researchers have postulated a similar mechanism on the apical side of the RPE (Sparrow et al., 2010).

Interestingly, Lrp5 protein is colocalized with Rbp1a protein at the microvilli of the RPE in the outer retina and Rbp1a directly binds to the C-terminal intracellular region of Lrp5 *in vitro* (Figures 4D and 4F). We also showed that *rbp1a* plays a role downstream of *lrp5* in a genetic study (Figures 3A and 3D). Previous studies show that LRP5 is involved in uptake of small molecules such as cholesterol (Fujino et al., 2003) and glucose (Chin et al., 2015); in the case of glucose, the mechanism is thought to be independent of the canonical LRP5 function where LRP5 is the frizzled co-receptor of WNT signaling. Furthermore, immunohistochemical approach using various human, mouse, and Rhesus monkey tissues suggests that LRP5 is expressed in such cell types that transport, store, and metabolize retinoids (Figueroa et al., 2000). In the visual cycle, RBP1 functions in transporting atROL in the cytoplasm at the microvilli of the RPE. Taken together, these results lead us to propose that LRP5 may be involved in the uptake of atROL at the microvilli of the RPE, and RBP1 is the downstream effector transporting atROL in the visual cycle (Figure 5, orange and light green in the right bottom, respectively). It would be of interest in future studies to examine the possible binding of atROL, its possible interaction with inter-photoreceptor retinol binding protein (IRBP), the possible presence of co-receptor(s) (e.g., peropsin [RRH] [Cook et al., 2017]), and other possible transport pathway(s) of atROL from photoreceptors (Figure 5, shown with "?").

In addition, the signals that were Rbp1a (and Lrp5) positive but MSN negative in the outer retina (Figures 4A, 4C, 4D, and S5) could be attributed to the processes of Müller cells (Figures S5E–S5G) (Bok et al., 1984; Bunt-Milam and Saari, 1983), which may suggest a possible involvement of RBP1 and LRP5 in the cone-specific visual cycle as well as the canonical visual cycle (Wang and Kefalov, 2011) and, therefore, would also be an interesting subject for future studies.

Insights into Understanding Functional Role(s) of Vertebrate Eys

In previous reports using zebrafish, immunohistochemical studies show that Eys protein is localized near connecting cilium/transition zone in photoreceptors (Liu et al., 2020; Messchaert et al., 2018; Yu et al., 2016) and the disruption of ciliary pocket in cones is observed in $eys^{-/-}$ (Yu et al., 2016). In *Drosophila*, a negative type of genetic interaction (Baryshnikova et al., 2010; Shen et al., 2017) is shown between *Eys* and *Prominin-1* (*Prom1*) genes in photoreceptors (Gurudev et al., 2014; Nie et al., 2012).

Based on the reports, we initially examined the possibility of a negative genetic interaction of *eys* and *prom1a* and/or *prom1b*, the zebrafish orthologs of *Prom1*, in the adult eye by qPCR using $eys^{-/-}$ and $prom1a^{-/-}$; $prom1b^{-/-}$ zebrafish eyes (Figures S1A, S1D, and S1E). Unfortunately, we were not able to observe any negative genetic interactions at least in the eye of zebrafish under the experimental conditions in this study (Figures 3B, 3C, and 3E). The results may reflect differences between vertebrate and invertebrate photoreceptors (Lamb, 2013). Future studies would be necessary to investigate whether their interaction at the genetic level could be observed in the zebrafish eyes having mutations at different positions on the *eys*, *prom1a*, and *prom1b* genes and/or by using photoreceptors. Confirmation of their binding at the protein level would be more rigorous, straightforward, and therefore promising.

On the other hand, we showed that the expression levels of the *rbp1a* gene and the Rbp1a protein are decreased in the $eys^{-/-}$ zebrafish eye for the first time, although the degrees were milder than those in the $eys^{+/-}$; $lrp5^{+/-}$ zebrafish eye. Genetic studies suggest that the remarkable decrease in the expression level of *rbp1a* is not induced by *lrp5* alone but that *eys* also contributes to the striking reduction (Figures 3A and S2F). Our present data may suggest a possible function of Eys in the visual cycle. Because it is believed that the ciliary pocket is the site of endocytosis and exocytosis (Ghossoub et al., 2011), it may be possible that Eys-deficiency may somehow impair release of atROL from cones. Whether this is related to dysfunction of the ciliary pocket or this is another possible contribution of Eys function is an interesting subject in future studies.

The Fate of Retinoid Metabolites in the Mutant Eyes and Possible Functional Implications of the Proteins

Because flaw of retinoids would be supposed to be impaired due to shortage of Rbp1a protein within the RPE, we postulate that atROL would probably be accumulated in the eye in the $eys^{+/-}$; $lrp5^{+/-}$ mutant compared with wild-type eye. In the $lrp5^{-/-}$ mutant eye, atROL may be accumulated in the eye also presumably as a result of failure of incorporation of atROL by the RPE. atROL may be accumulated between photoreceptors and RPE (i.e., inter-photoreceptor matrix, IPM) in the $lrp5^{-/-}$ mutant. In the $eys^{-/-}$ mutant eye, it may be possible that atROL may be accumulated in the eye also if Lrp5 and Eys would physically

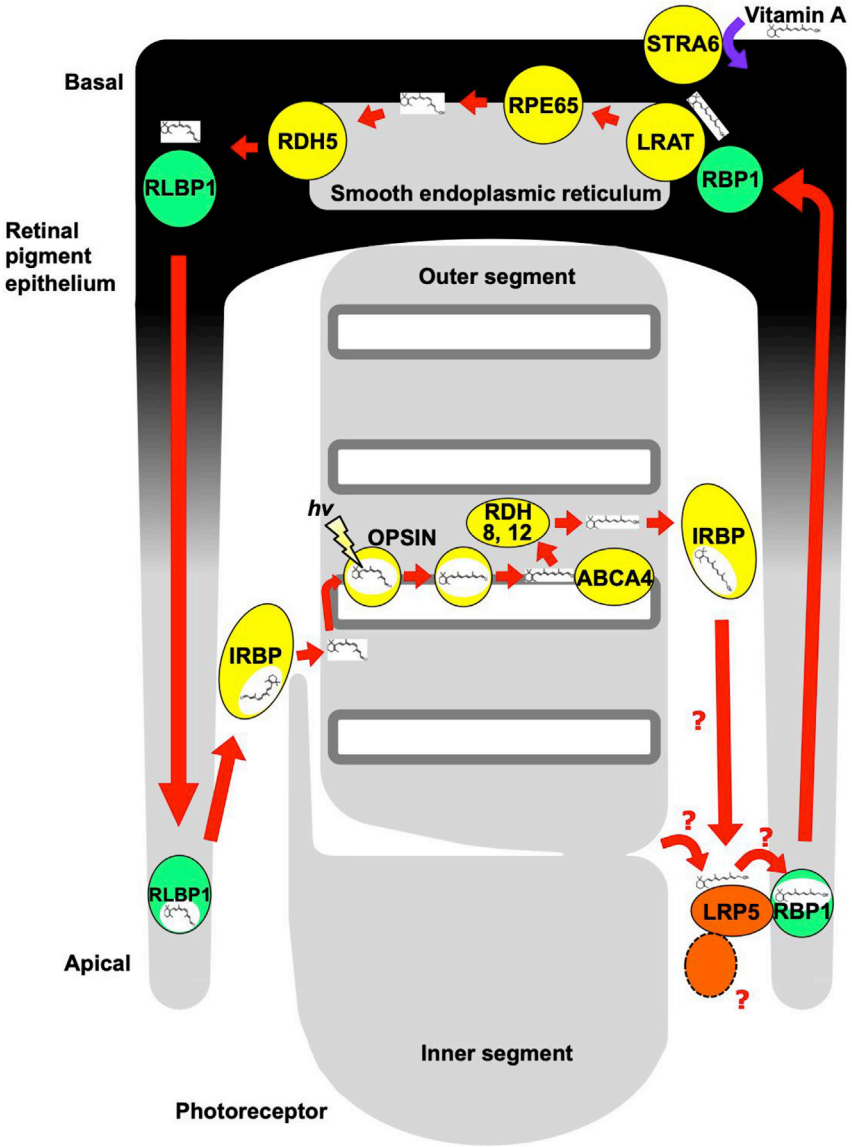

Figure 5. A Proposed Model of LRP5 Function in the Visual Cycle

LRP5 protein (shown in orange in right bottom) is a strong candidate for the receptor of atROL by forming a complex with RBP1 protein (the transporter of atROL, shown in light green in right bottom) and may be involved in the uptake of atROL in the RPE in the visual cycle. The flow of retinoids is shown by red arrows and the unknown possible interactions are indicated with "?". atROL, all-*trans* retinol; ABCA4, ATP binding cassette subfamily A member 4; IRBP, inter-photoreceptor retinol binding protein (also known as RBP3, retinol binding protein 3); LRAT, lecithin retinol acyltransferase; LRP5, LDL receptor related protein 5; RBP1, retinol binding protein 1 (also known as CRBP, cellular retinol binding protein); RDH, retinol dehydrogenase; RLBP1, retinaldehyde binding protein 1 (also known as CRALBP, cellular retinal binding protein); RPE65, retinoid isomerohydrolase RPE65; STRA6, stimulated by retinoic acid gene 6.

interact with each other because atROL could not be incorporated into the RPE from IPM. Alternatively, it may be possible that atROL may be accumulated in photoreceptors if Eys would be involved in the retinoid metabolism within photoreceptors because atROL could not correctly be released from photoreceptors.

In the present study, we shed light on the decade-long missing link in vision by analyzing the digenic *eys*$^{+/-}$; *lrp5*$^{+/-}$ mutations. With recent great advances and lower costs of NGS technology, which have made it far easier to detect digenic (or even more, i.e., polygenic) mutations, a combination of detection and comprehensive analysis of polygenic inheritance could be a powerful tool to dissect molecular networks such as

protein-protein interactions and protein complexes not only in vision but also in other fields of biology and medicine.

Limitations of the Study

We did not examine electroretinogram (ERG) in the *eys*$^{+/-}$; *lrp5*$^{+/-}$ zebrafish because detailed examination of electrophysiology of the mutant would have been secondary support for the main conclusions of this study. We did not examine retinoid contents in the *eys*$^{+/-}$; *lrp5*$^{+/-}$ zebrafish eye, partly due to travel limitations under the current circumstances, and therefore did not include such data. In addition, the short variants, EYS-1-3 and EYS-1-4 (Takita et al., 2019), are not affected in the *eys*^{sa31957} mutants, and therefore, other possible function(s) for EYS owing to the variants are not unnecessarily omitted.

Resource Availability

Lead Contact

Further information and requests should be directed to and will be fulfilled by the corresponding author, Yuko Seko (seko-yuko@rehab.go.jp).

Data Availability

Microarray data are deposited in the GEO with the accession number GSE160663. Nucleotide sequence of zebrafish *rbp1a* is deposited in the DDBJ with the accession number LC579941.

METHODS

All methods can be found in the accompanying Transparent Methods supplemental file.

SUPPLEMENTAL INFORMATION

Supplemental Information can be found online at https://doi.org/10.1016/j.isci.2020.101762.

ACKNOWLEDGMENTS

We thank Drs. Y. Sawada, M. Nagao, T. Maekawa, and S. Toyama (NRCPD) for their kind equipment sharing. We also thank Prof. Y. Fukada and Lecturer D. Kojima (University of Tokyo) for the puller sharing and Mrs. N. Nogami (NRCPD) for technical assistance in the qPCR, genotyping, and DNA sequencing experiments. This work was supported by JSPS KAKENHI Grant Numbers 17K16995 (to S.T.), 20K18364 (to S.T.), 15H04998 (to Y.S.), and 20H03845 (to Y.S.). The zebrafish mutant lines, *eys*^{sa31957}, *lrp5*^{sa11097}, and *prom1b*^{sa13905} were obtained from the ZIRC.

AUTHOR CONTRIBUTIONS

S.T. conceived and designed the study, performed the experiments, analyzed the data, and wrote the draft. Y.S. supervised the study. S.T. and Y.S. wrote the manuscript.

DECLARATION OF INTERESTS

The authors declare no competing interests.

Received: June 8, 2020
Revised: September 17, 2020
Accepted: October 30, 2020
Published: December 18, 2020

REFERENCES

Abd El-Aziz, M.M., Barragan, I., O'Driscoll, C.A., Goodstadt, L., Prigmore, E., Borrego, S., Mena, M., Pieras, J.I., El-Ashry, M.F., Safieh, L.A., et al. (2008). EYS, encoding an ortholog of Drosophila spacemaker, is mutated in autosomal recessive retinitis pigmentosa. Nat. Genet. *40*, 1285–1287.

Bander, N.H., Yao, D., Liu, H., Chen, Y.T., Steiner, M., Zuccaro, W., and Moy, P. (1997). MHC class I and II expression in prostate carcinoma and modulation by interferon-alpha and -gamma. Prostate *33*, 233–239.

Baryshnikova, A., Costanzo, M., Kim, Y., Ding, H., Koh, J., Toufighi, K., Youn, J.Y., Ou, J., San Luis, B.J., Bandyopadhyay, S., et al. (2010). Quantitative analysis of fitness and genetic interactions in yeast on a genome scale. Nat. Methods *7*, 1017–1024.

Berryman, M., Franck, Z., and Bretscher, A. (1993). Ezrin is concentrated in the apical microvilli of a wide variety of epithelial cells whereas moesin is found primarily in endothelial cells. J. Cell Sci *105* (Pt 4), 1025–1043.

Bok, D., Ong, D.E., and Chytil, F. (1984). Immunocytochemical localization of cellular retinol binding protein in the rat retina. Invest. Ophthalmol. Vis. Sci. *25*, 877–883.

Bonilha, V.L., Bhattacharya, S.K., West, K.A., Sun, J., Crabb, J.W., Rayborn, M.E., and Hollyfield, J.G. (2004). Proteomic characterization of isolated retinal pigment epithelium microvilli. Mol. Cell Proteomics *3*, 1119–1127.

Bunt-Milam, A.H., and Saari, J.C. (1983). Immunocytochemical localization of two retinoid-binding proteins in vertebrate retina. J. Cell Biol. *97*, 703–712.

Chin, E.N., Martin, J.A., Kim, S., Fakhraldeen, S.A., and Alexander, C.M. (2015). Lrp5 has a Wnt-independent role in glucose uptake and growth for mammary epithelial cells. Mol. Cell Biol. *36*, 871–885.

Collin, R.W., Littink, K.W., Klevering, B.J., van den Born, L.I., Koenekoop, R.K., Zonneveld, M.N., Blokland, E.A., Strom, T.M., Hoyng, C.B., den Hollander, A.I., and Cremers, F.P. (2008). Identification of a 2 Mb human ortholog of Drosophila eyes shut/spacemaker that is mutated in patients with retinitis pigmentosa. Am. J. Hum. Genet. *83*, 594–603.

Cook, J.D., Ng, S.Y., Lloyd, M., Eddington, S., Sun, H., Nathans, J., Bok, D., Radu, R.A., and Travis, G.H. (2017). Peropsin modulates transit of vitamin A from retina to retinal pigment epithelium. J. Biol. Chem. *292*, 21407–21416.

Figueroa, D.J., Hess, J.F., Ky, B., Brown, S.D., Sandig, V., Hermanowski-Vosatka, A., Twells, R.C., Todd, J.A., and Austin, C.P. (2000). Expression of the type I diabetes-associated gene LRP5 in macrophages, vitamin A system cells, and the Islets of Langerhans suggests multiple potential roles in diabetes. J. Histochem. Cytochem. *48*, 1357–1368.

Fujino, T., Asaba, H., Kang, M.J., Ikeda, Y., Sone, H., Takada, S., Kim, D.H., Ioka, R.X., Ono, M., Tomoyori, H., et al. (2003). Low-density lipoprotein receptor-related protein 5 (LRP5) is essential for normal cholesterol metabolism and glucose-induced insulin secretion. Proc. Natl. Acad. Sci. U S A *100*, 229–234.

Gao, F.J., Zhang, S.H., Chen, J.Y., Xu, G.Z., and Wu, J.H. (2017). Digenic heterozygous mutations in EYS/LRP5 in a Chinese family with retinitis pigmentosa. Int. J. Ophthalmol. *10*, 325–328.

Ghossoub, R., Molla-Herman, A., Bastin, P., and Benmerah, A. (2011). The ciliary pocket: a once-forgotten membrane domain at the base of cilia. Biol. Cell *103*, 131–144.

Ghyselinck, N.B., Bavik, C., Sapin, V., Mark, M., Bonnier, D., Hindelang, C., Dierich, A., Nilsson, C.B., Hakansson, H., Sauvant, P., et al. (1999). Cellular retinol-binding protein I is essential for vitamin A homeostasis. EMBO J. *18*, 4903–4914.

Goldberg, A.F., and Molday, R.S. (1996). Defective subunit assembly underlies a digenic form of retinitis pigmentosa linked to mutations in peripherin/rds and rom-1. Proc. Natl. Acad. Sci. U S A *93*, 13726–13730.

Gong, Y., Slee, R.B., Fukai, N., Rawadi, G., Roman-Roman, S., Reginato, A.M., Wang, H., Cundy, T., Glorieux, F.H., Lev, D., et al. (2001). LDL receptor-related protein 5 (LRP5) affects bone accrual and eye development. Cell *107*, 513–523.

Gurudev, N., Yuan, M., and Knust, E. (2014). chaoptin, prominin, eyes shut and crumbs form a genetic network controlling the apical compartment of Drosophila photoreceptor cells. Biol. Open *3*, 332–341.

Holling, T.M., Schooten, E., and van Den Elsen, P.J. (2004). Function and regulation of MHC class II molecules in T-lymphocytes: of mice and men. Hum. Immunol. *65*, 282–290.

Hosono, K., Ishigami, C., Takahashi, M., Park, D.H., Hirami, Y., Nakanishi, H., Ueno, S., Yokoi, T., Hikoya, A., Fujita, T., et al. (2012). Two novel mutations in the EYS gene are possible major causes of autosomal recessive retinitis pigmentosa in the Japanese population. PLoS One *7*, e31036.

Huang, J., Possin, D.E., and Saari, J.C. (2009). Localizations of visual cycle components in retinal pigment epithelium. Mol. Vis. *15*, 223–234.

Iwanami, M., Oshikawa, M., Nishida, T., Nakadomari, S., and Kato, S. (2012). High prevalence of mutations in the EYS gene in Japanese patients with autosomal recessive retinitis pigmentosa. Invest. Ophthalmol. Vis. Sci. *53*, 1033–1040.

Kajiwara, K., Berson, E.L., and Dryja, T.P. (1994). Digenic retinitis pigmentosa due to mutations at the unlinked peripherin/RDS and ROM1 loci. Science *264*, 1604–1608.

Katagiri, S., Akahori, M., Hayashi, T., Yoshitake, K., Gekka, T., Ikeo, K., Tsuneoka, H., and Iwata, T. (2014). Autosomal recessive cone-rod dystrophy associated with compound heterozygous mutations in the EYS gene. Doc Ophthalmol. *128*, 211–217.

Kawaguchi, R., Yu, J., Honda, J., Hu, J., Whitelegge, J., Ping, P., Wiita, P., Bok, D., and Sun, H. (2007). A membrane receptor for retinol binding protein mediates cellular uptake of vitamin A. Science *315*, 820–825.

Kawamura, S., and Tachibanaki, S. (2008). Rod and cone photoreceptors: molecular basis of the difference in their physiology. Comp. Biochem. Physiol. A. Mol. Integr. Physiol. *150*, 369–377.

Kim, N., Stiegler, A.L., Cameron, T.O., Hallock, P.T., Gomez, A.M., Huang, J.H., Hubbard, S.R., Dustin, M.L., and Burden, S.J. (2008). Lrp4 is a receptor for Agrin and forms a complex with MuSK. Cell *135*, 334–342.

Lamb, T.D. (2013). Evolution of phototransduction, vertebrate photoreceptors and retina. Prog. Retin. Eye Res. *36*, 52–119.

Li, J.K., Li, Y., Zhang, X., Chen, C.L., Rao, Y.Q., Fei, P., Zhang, Q., Zhao, P., and Li, J. (2018). Spectrum of variants in 389 Chinese probands with familial exudative vitreoretinopathy. Invest. Ophthalmol. Vis. Sci. *59*, 5368–5381.

Liu, Y., Yu, M., Shang, X., Nguyen, M.H.H., Balakrishnan, S., Sager, R., and Hu, H. (2020). Eyes shut homolog (EYS) interacts with matriglycan of O-mannosyl glycans whose deficiency results in EYS mislocalization and degeneration of photoreceptors. Sci. Rep. *10*, 7795.

Lu, Z., Hu, X., Liu, F., Soares, D.C., Liu, X., Yu, S., Gao, M., Han, S., Qin, Y., Li, C., et al. (2017). Ablation of EYS in zebrafish causes mislocalisation of outer segment proteins, F-actin disruption and cone-rod dystrophy. Sci. Rep. *7*, 46098.

Messchaert, M., Dona, M., Broekman, S., Peters, T.A., Corral-Serrano, J.C., Slijkerman, R.W.N., van Wijk, E., and Collin, R.W.J. (2018). Eyes shut homolog is important for the maintenance of photoreceptor morphology and visual function in zebrafish. PLoS One *13*, e0200789.

Nie, J., Mahato, S., Mustill, W., Tipping, C., Bhattacharya, S.S., and Zelhof, A.C. (2012). Cross species analysis of Prominin reveals a conserved cellular role in invertebrate and vertebrate photoreceptor cells. Dev. Biol. *371*, 312–320.

Pierrache, L.H.M., Messchaert, M., Thiadens, A., Haer-Wigman, L., de Jong-Hesse, Y., van Zelst-Stams, W.A.G., Collin, R.W.J., Klaver, C.C.W., and van den Born, L.I. (2019). Extending the spectrum of EYS-associated retinal disease to macular dystrophy. Invest. Ophthalmol. Vis. Sci. *60*, 2049–2063.

Shen, J.P., Zhao, D., Sasik, R., Luebeck, J., Birmingham, A., Bojorquez-Gomez, A., Licon, K., Klepper, K., Pekin, D., Beckett, A.N., et al. (2017). Combinatorial CRISPR-Cas9 screens for de novo mapping of genetic interactions. Nat. Methods *14*, 573–576.

Sparrow, J.R., Hicks, D., and Hamel, C.P. (2010). The retinal pigment epithelium in health and disease. Curr. Mol. Med. *10*, 802–823.

Takita, S., Miyamoto-Matsui, K., and Seko, Y. (2019). Intra- and interspecies comparison of EYS transcripts highlights its characteristics in the eye. FASEB J. *33*, 9422–9433.

Tamai, K., Semenov, M., Kato, Y., Spokony, R., Liu, C., Katsuyama, Y., Hess, F., Saint-Jeannet, J.P., and He, X. (2000). LDL-receptor-related proteins in Wnt signal transduction. Nature *407*, 530–535.

Wang, J.S., and Kefalov, V.J. (2011). The cone-specific visual cycle. Prog. Retin. Eye Res. *30*, 115–128.

Yang, H., Li, S., Xiao, X., Wang, P., Guo, X., and Zhang, Q. (2012). Identification of FZD4 and LRP5 mutations in 11 of 49 families with familial exudative vitreoretinopathy. Mol. Vis. *18*, 2438–2446.

Yu, M., Liu, Y., Li, J., Natale, B.N., Cao, S., Wang, D., Amack, J.D., and Hu, H. (2016). Eyes shut homolog is required for maintaining the ciliary pocket and survival of photoreceptors in zebrafish. Biol. Open *5*, 1662–1673.

Zhang, W., Coldefy, A.S., Hubbard, S.R., and Burden, S.J. (2011). Agrin binds to the N-terminal region of Lrp4 protein and stimulates association between Lrp4 and the first immunoglobulin-like domain in muscle-specific kinase (MuSK). J. Biol. Chem. *286*, 40624–40630.

iScience, Volume *23*

Supplemental Information

eys$^{+/-}$; *lrp5*$^{+/-}$ Zebrafish Reveals Lrp5 Can Be the Receptor of Retinol in the Visual Cycle

Shimpei Takita and Yuko Seko

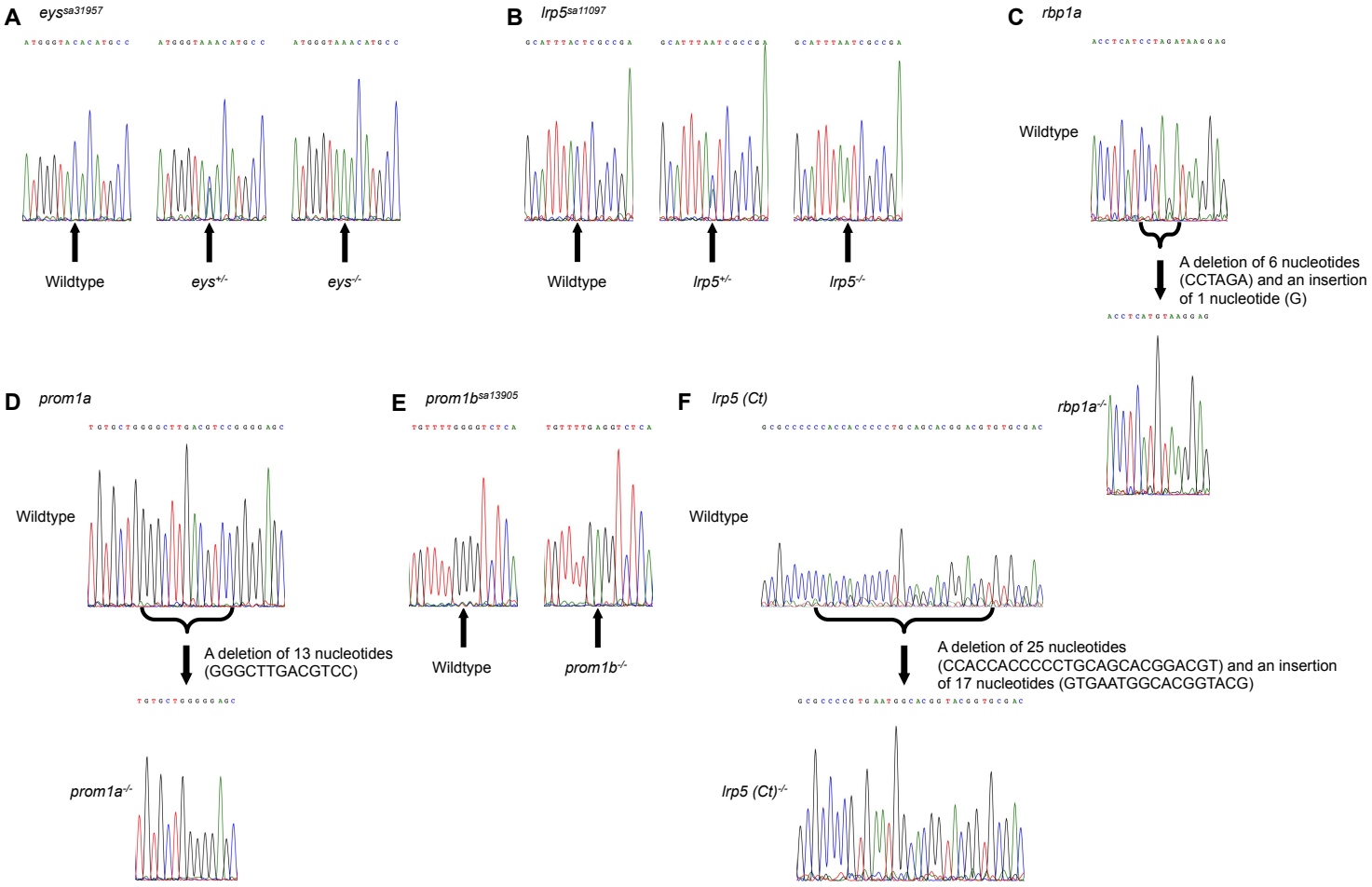

Figure S1. Zebrafish mutant lines used. Related to Figures 1-4 and S2-S4.

(A) *eys*^{sa31957} carries a nonsense mutation (premature stop codon) C>A (arrows, Y2440X in EYS-1-1 (Takita et al., 2019)).

(B) *lrp5*^{sa11097} carries a nonsense mutation C>A (arrows, Y284X in Lrp5 variant 1 (Lrp5-1; XP_009296098.1)).

(C) *rbp1*$^{-/-}$ carries a deletion of 6 nucleotides (CCTAGA, nucleotide position 169-174 of NM_001114899.1) and an insertion of a nucleotide (G) in the deleted region resulting in a frameshift after the first 38 amino acids of NP_001108371.1.

(D) *prom1a*$^{-/-}$ carries a deletion of 13 nucleotides (nucleotide position 358-370 of XM_021480968.1 or transcript variant 1 of *prom1a* (*prom1a-1*)) resulting in a frameshift immediately after the start codon (first 13 amino acids of XP_021336643.1).

(E) *prom1b*^{sa13905} carries a nonsense mutation G>A (arrows, position 354 of XM_021481233.1 or transcript variant 1 of *prom1b* (*prom1b-1*)) resulting in a truncation after the first 14 amino acids in the signal peptide sequence region (W15X in Prom1b variant 1 (Prom1b-1; XP_021336908.1)).

(F) *lrp5 (Ct)*$^{-/-}$ carries a deletion of 25 nucleotides (CCACCACCCCCTGCAGCACAGACGT, nucleotide position 4761-4785 of XM_009297823.3 or transcript variant 1 of *lrp5* (*lrp5-1*)) and an insertion of 17 nucleotides (GTGAATGGCACGGTACG) resulting in frameshift after position 1538 of Lrp5-1.

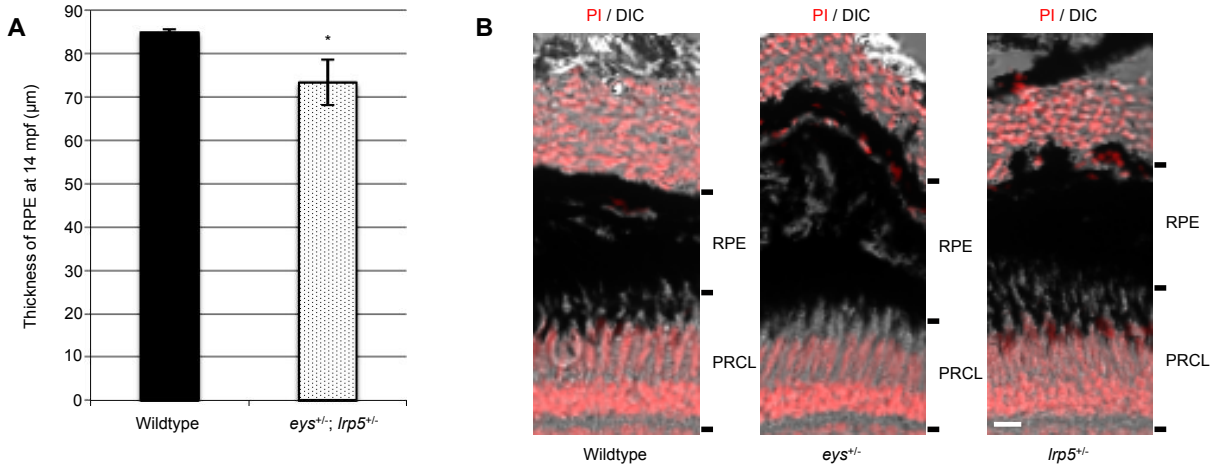
A
Thickness of RPE at 14 mpf (µm)
90
80
70
60
50
40
30
20
10
0
*
Wildtype
eys+/-; lrp5+/-
B
PI / DIC
PI / DIC
PI / DIC
RPE
PRCL
RPE
PRCL
RPE
PRCL
Wildtype
eys+/-
lrp5+/-

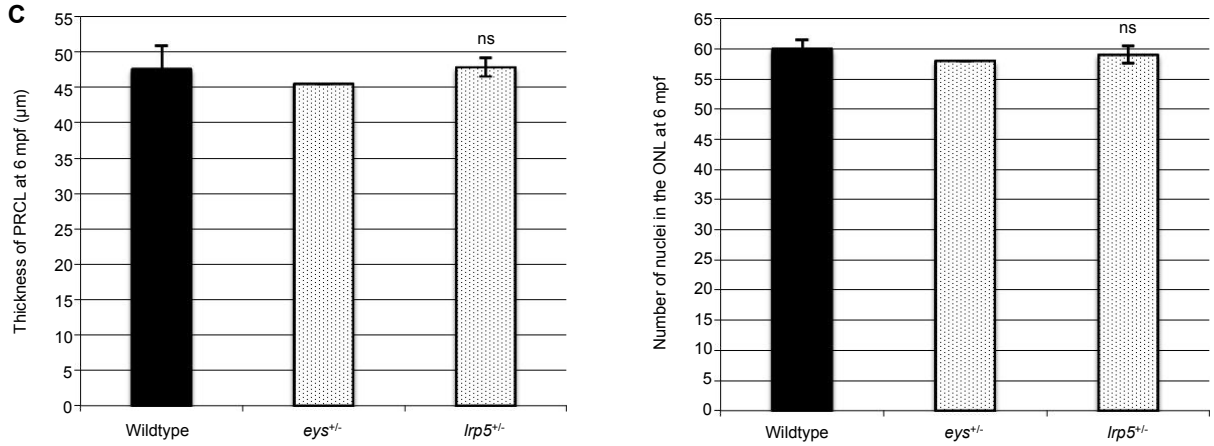
C
Thickness of PRCL at 6 mpf (µm)
55
50
45
40
35
30
25
20
15
10
5
0
ns
Wildtype
eys+/-
lrp5+/-
Number of nuclei in the ONL at 6 mpf
65
60
55
50
45
40
35
30
25
20
15
10
5
0
ns
Wildtype
eys+/-
lrp5+/-

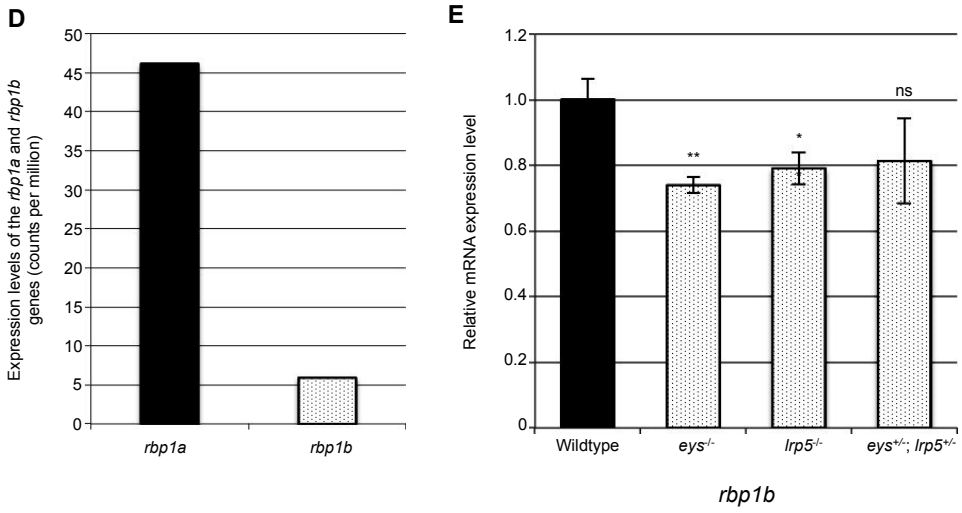
D
Expression levels of the rbp1a and rbp1b genes (counts per million)
50
45
40
35
30
25
20
15
10
5
0
rbp1a
rbp1b
E
Relative mRNA expression level
1.2
1.0
0.8
0.6
0.4
0.2
0
**
*
ns
Wildtype
eys-/-
lrp5-/-
eys+/-; lrp5+/-
rbp1b

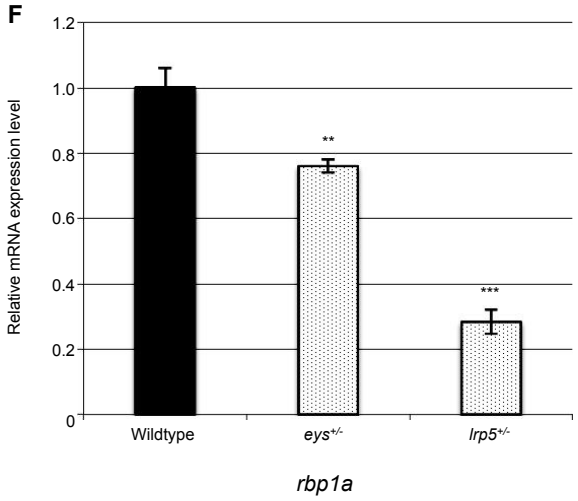
F
Relative mRNA expression level
1.2
1.0
0.8
0.6
0.4
0.2
0
**
***
Wildtype
eys+/-
lrp5+/-
rbp1a

Figure S2. Effects of single and digenic mutations on the retina and change in the expression levels of *rbp1a* (*rbp1.2*) and *rbp1b* (*rbp1.1*). Related to Figures 1, 2, and 3.

(A) The RPE layer was 14% thinner in the $eys^{+/-}$; $lrp5^{+/-}$ eye (wildtype, 84.9 ± 0.7 μm; $eys^{+/-}$; $lrp5^{+/-}$ mutants 73.3 ± 5.2, n = 3). Data are represented as mean ± SD. *p = 0.0186.

(B and C) Significant changes in the thickness of PRCL or number of nuclei in the ONL were not observed among wildtype, $eys^{+/-}$, and $lrp5^{+/-}$ zebrafish. (47.59 ± 3.3 μm for wildtype, 45.5 μm for $eys^{+/-}$, and 47.83 ± 1.3 μm for $lrp5^{+/-}$ PRCLs; 60 ± 1.4 for wildtype, 58 for $eys^{+/-}$, and 59 ± 1.4 for $lrp5^{+/-}$ ONLs; n = 2, 1, and 2 for wildtype, $eys^{+/-}$, and $lrp5^{+/-}$ zebrafish, respectively). Scale bar, 10 μm. Data are represented as mean ± SD. NS, not significant.

(D) The expression levels of the *rbp1a* (*rbp1.2*) and *rbp1b* (*rbp1.1*) genes by cap analysis of gene expression (CAGE) (counts per million) was 46.16 and 5.92, respectively.

(E) The expression levels of *rbp1b* (*rbp1.1*) was about 20% reduced in the $eys^{-/-}$, $lrp5^{-/-}$, and $eys^{+/-}$; $lrp5^{+/-}$ eyes ($eys^{-/-}$, 74.0 ± 2.5%; $lrp5^{-/-}$, 79.1 ± 4.8% ; $eys^{+/-}$; $lrp5^{+/-}$,81.4 ± 12.9%, n=3) by qPCR. Data are represented as mean ± SD.

(F) The expression levels of *rbp1a* (*rbp1.2*) were 28.4 ± 3.6% in the $lrp5^{+/-}$ eye and 76.0 ± 1.9% in the $eys^{+/-}$ eye compared to the wildtype (n = 3). Data are represented as mean ± SD. **$p < 0.005$, **$p < 0.0001$.

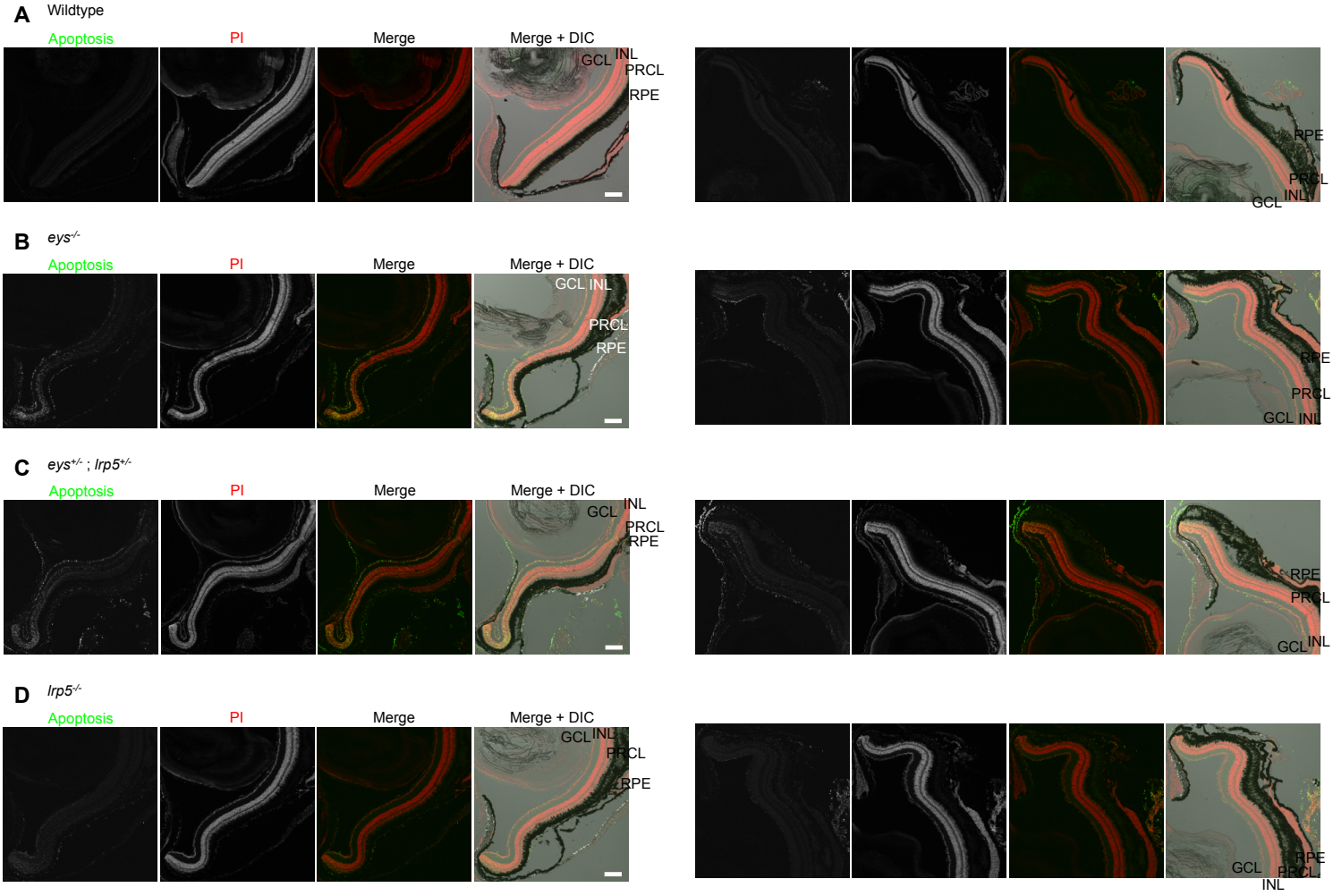

Figure S3. Photoreceptor degeneration in the digenic *eys*$^{+/-}$; *lrp5*$^{+/-}$ zebrafish at 8 mpf detected by TUNEL staining. Related to Figure 1.

(A-D) Apoptotic cells (green) were observed in the photoreceptor cell layer (PRCL) in the digenic *eys*$^{+/-}$; *lrp5*$^{+/-}$ zebrafish (C) while no apoptotic cells were observed in PRCL in wildtype zebrafish (A). Panels on the left half show central-ventral regions and panels on the right half show central-dorsal regions. Peripheral regions are intensely labeled. Apoptotic cells were also observed in the PRCLs of the *eys*$^{-/-}$ and *lrp5*$^{-/-}$ eyes (B and D respectively). Nuclei were stained with propidium iodide (PI) (red). GCL, ganglion cell layer; INL, inner nuclear layer; PRCL, photoreceptor cell layer; RPE, retinal pigment epithelium. Scale bars, 100 μm.

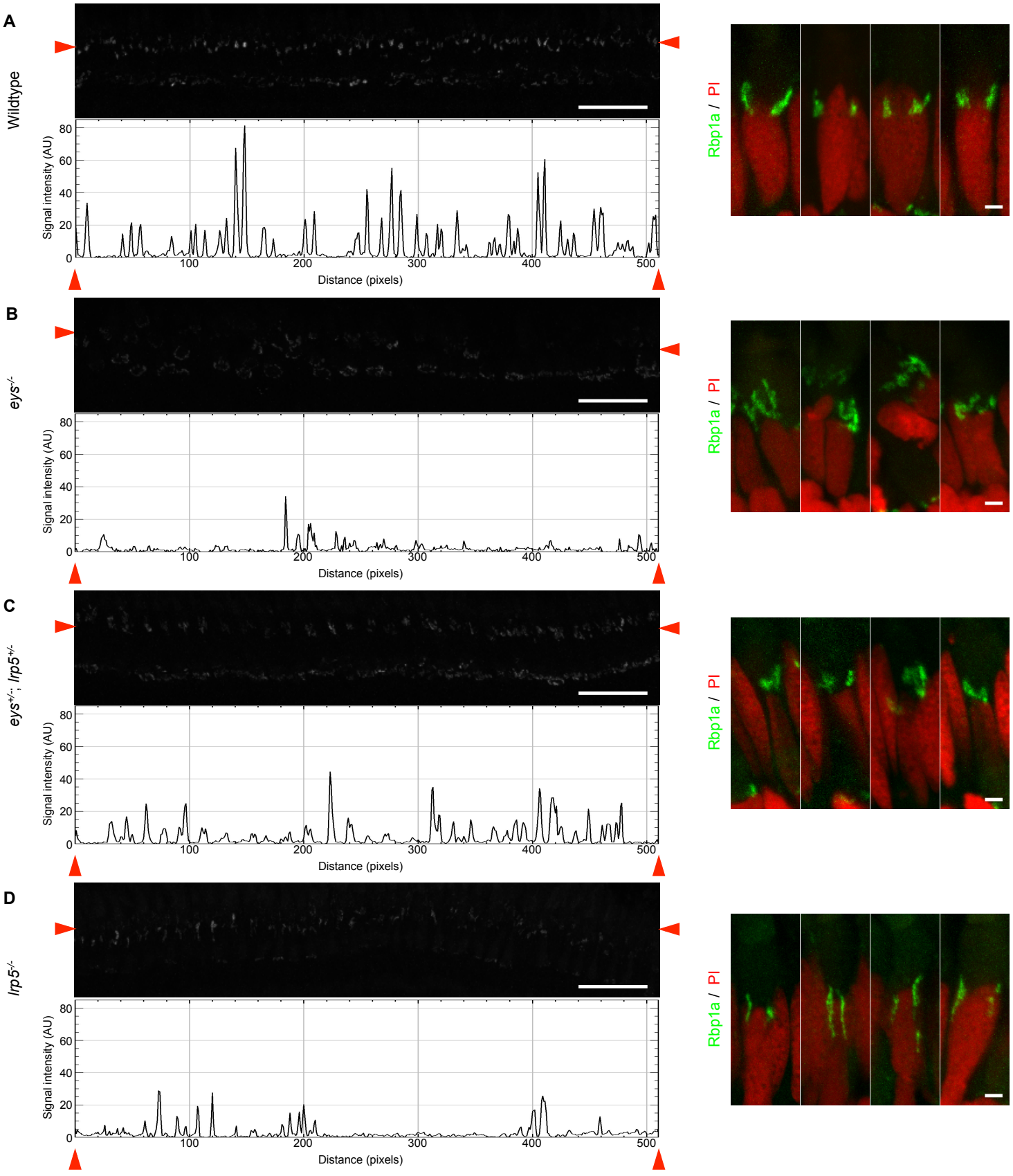
A
Wildtype
Signal intensity (AU)
Distance (pixels)
Rbp1a / PI
B
eys-/-
Signal intensity (AU)
Distance (pixels)
Rbp1a / PI
C
eys+/-; lrp5+/-
Signal intensity (AU)
Distance (pixels)
Rbp1a / PI
D
lrp5-/-
Signal intensity (AU)
Distance (pixels)
Rbp1a / PI

Figure S4. Immunohistochemical analysis of Rbp1a expression in the digenic *eys*$^{+/-}$; *lrp5*$^{+/-}$ zebrafish adult eyes. Related to Figure 2.

(A-D) Upper left panels and their plot profiles (left and right ends are indicated by red arrowheads) show the signal for Rbp1a. Both the signal intensity and the number of spots were decreased in the digenic *eys*$^{+/-}$; *lrp5*$^{+/-}$ eyes (C) compared to wildtype eyes (A). The expression levels of Rbp1a protein were also decreased in the *eys*$^{-/-}$ and *lrp5*$^{-/-}$ eyes (B and D, respectively). In the *eys*$^{-/-}$ eyes, the number of Rbp1a-positive microvilli appeared to be more affected than the signal intensity. The fine structures of the concentrated regions indicated by Rbp1a (green) may suggest that the structures underwent slightly differently alteration between the mutant retinas (right panels). Nuclei were stained with propidium iodide (PI) (red). Scale bars, 20 μm in left panels and 2 μm in right panels.

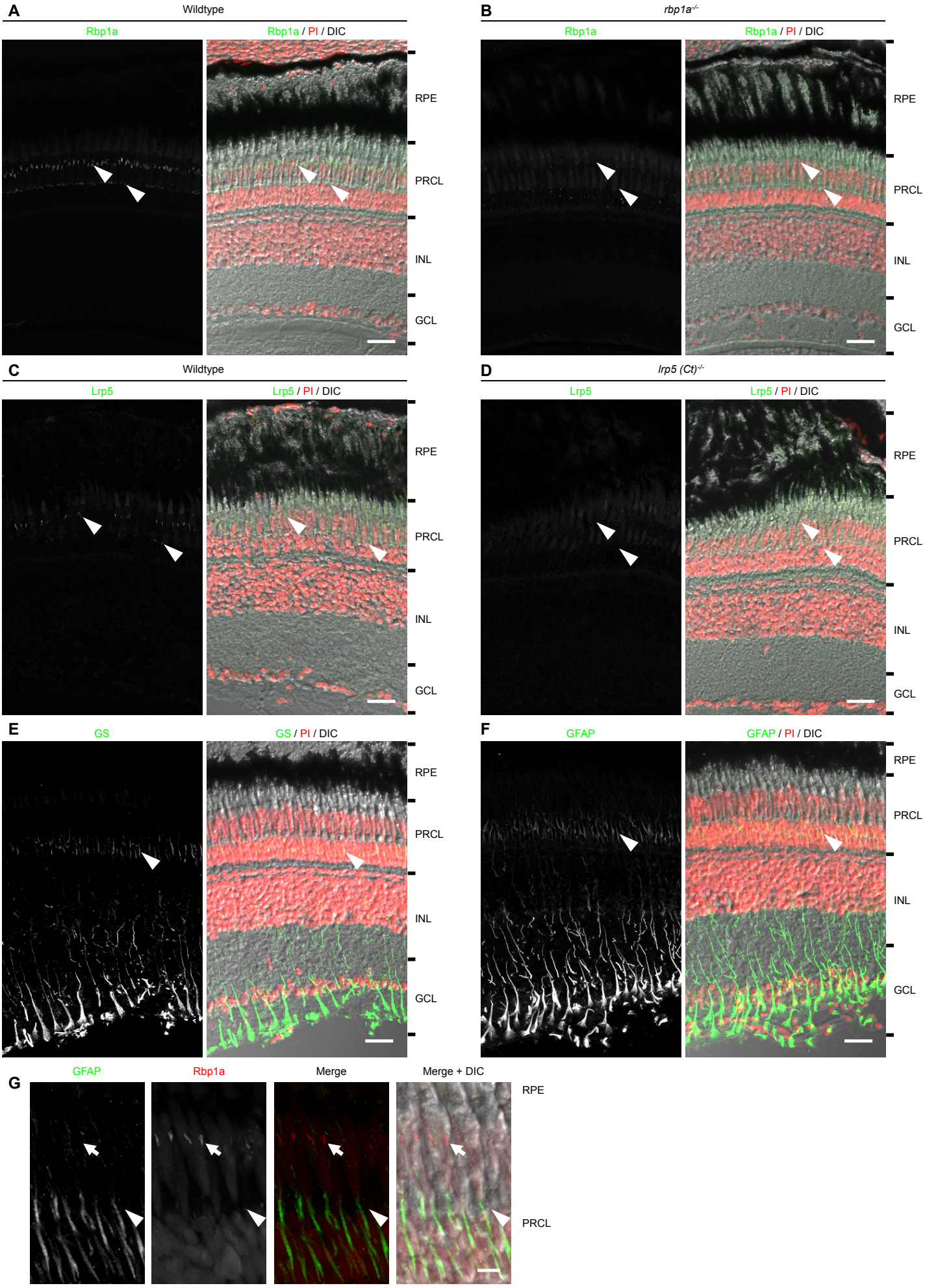
A
Wildtype
Rbp1a
Rbp1a / PI / DIC
RPE
PRCL
INL
GCL
B
rbp1a-/-
Rbp1a
Rbp1a / PI / DIC
RPE
PRCL
INL
GCL
C
Wildtype
Lrp5
Lrp5 / PI / DIC
RPE
PRCL
INL
GCL
D
lrp5 (Ct)-/-
Lrp5
Lrp5 / PI / DIC
RPE
PRCL
INL
GCL
E
GS
GS / PI / DIC
RPE
PRCL
INL
GCL
F
GFAP
GFAP / PI / DIC
RPE
PRCL
INL
GCL
G
GFAP
Rbp1a
Merge
Merge + DIC
RPE
PRCL

Figure S5. Validation of specificity of the anti-Rbp1a and anti-Lrp5 antibodies and clarification of Müller glial processes in the zebrafish adult eyes. Related to Figure 4.

(A and B) Immunopositive signals (green) were detected in the outer retina in wildtype eyes (A, arrowheads). Immunopositive signals were not detected in the same region (B, arrowheads) nor in other region in the outer retina in the *rbp1a*$^{-/-}$ eyes. Nuclei were stained with propidium iodide (PI) (red).

(C and D) Immunopositive signals (green) were detected in the outer retina in wildtype eyes (C, arrowheads). Immunopositive signals were not detected in the same region (D, arrowheads) nor in other region in the outer retina in the *lrp5 (Ct)*$^{-/-}$ eyes.

(E - G) The processes of Müller cells were stained with anti-GFAP and anti-GS antibodies. The processes were also co-stained with the antibody to Rbp1a to compare the location within the outer retina. Arrows and arrowheads indicate the location of the microvilli of RPE cells and the processes of Müller cells, respectively. Nuclei were stained with PI (red). Ct, C-terminal region; DIC, differential interference contrast; GFAP, fibrillary acidic protein; GS, glutamine synthetase. Scale bars, 20 μm in A, B, C, D, E, and F, and 5 μm in G.

Table S1. Primer sequences for screening and genotyping of zebrafish mutants. Related to Figures 1, 2, and 3.

eys	
Dreys_Fw7530	GTTTCATGCTCTAGGAGGGCCA
Dreys_g_Rev1	ACGGTAATATGCAAAAGTGCGT
lrp5	
Drlrp5_g_Fw1	AGGATCCACAAATGCTACAGATGTT
Drlrp5_g_Rev1	ACCTGACCTGAGTGCAAAACAG
rbp1a	
Drrbp1_Fw_g1	ACGTGGATGCATTTTGTAGAGT
Drrbp1_Rev243	ATGTCGTAGTTCCTAAATGTGGTT
prom1a	
prom1a_Fw190	TGATCATCATGACTCGCTCGCC
prom1a_Rev538	GTTGGGCTGAACCACAAAGAGG
prom1b	
Drprom1b_Fw30	AGGTCACACAAACACTCAGCTC
Drprom1b_Rev504	CCCCATGGGACCTGGTTCATAA

Table S2. Primer sequences for qPCR. Related to Figure 3.

actb2	
Dractb2_Fw282	GAGGTATCCTGACCCTGAAGTA
Dractb2_Rev361	GTGATGCCAGATCTTCTCCATA
rbp1a	
Drrbp1_Fw116	AACTGGGAAGAGGATAAGTTGG
Drrbp1_Rev424	ACAGACTCTCATTTCCACATGT
rbp1b	
Drrbp1b_Fw115	GGAAAATGATCTCCAACAACAAC
Drrbp1b_Rev296	CTCCTGACCAACTACAAAGTCC
lrp5	
Drlrp5_Fw757	ACTCACCATTGACCTGGACGAG
Drlrp5_Rev1210	AGTGCGACGAGCAAGTAAAAGC
prom1a	
Drprom1a_Fw1674	TTACCCTGTGCTGTATGATTGT
Drprom1a_Rev1869	AAAGCTGTTATGACTCCCATGA
prom1b	
Drprom1b_Fw1489	AGGGAACAGACTAAAGGGATTG
Drprom1b_Rev1570	AACCAATAATCTCTGCACCTGA
eys (5' region)	
Dreys_Fw1586	CTTGTCTCAACGGTGGCATCTG
DrEYS_Rev1816	AGGCTAAGCATGCGTTCTCCAA
eys (3' region)	
Dreys_Fw7856	CTCCCATCAACATAAGGCACAG
Dreys_Rev8096	ACATCTAACTCTTTCGGAGACTG
eys (splice variant 3)	
Dreys_splicing_Fw5646	GTGTGTGGCTGAAGTCACCGTTA
Dreys_splicing_Rev1	GGAAAACAGAAACATCTCAGGCTTT

Table S3. Primer sequences for cloning of zebrafish *rbp1a* and *lrp5* genes. Related to Figure 4.

rbp1a	
Drrbp1_Fw7	ATGTTGAAACATCAGCGCA
Drrbp1_Rev888	AAGAATTGTGCAGGTTTTTATTG
lrp5	
Drlrp5_EcoRI_F4370-2	TCGGTACCGCTCTTCGAATTCCAGAGAGTCGTGTG
Drlrp5_Ct5_Rev	CAATGCCTGAGGAGTCTGTGCAGGGCG

Transparent Methods

Zebrafish care

All experiments with zebrafish (*Danio rerio*) in this study were performed in accordance with the institutional guidelines and all experimental protocols were approved by the Institutional Animal Care and Use Committee of National Rehabilitation Center for Persons with Disabilities Research Institute. The fish were kept under 14 hr light/10 hr dark cycle at 28.5°C. When necessary, the fish were anesthetized by putting them in ice-chilled water and decapitated during the light period.

Generation of *eys*$^{+/-}$; *lrp5*$^{+/-}$, *eys*$^{-/-}$, and *lrp5*$^{-/-}$ zebrafish

The *eys*^{sa31957} (*eys*$^{+/-}$) and *lrp5*^{sa11097} (*lrp5*$^{+/-}$) mutant lines (isolated by Zebrafish Mutation Project (https://www.sanger.ac.uk/resources/zebrafish/zmp/) (Kettleborough et al., 2013)) were obtained from the Zebrafish International Resource Center (ZIRC). *eys*^{sa31957} carries a nonsense mutation (premature stop codon) C>A (Figure S1A; Y2440X in EYS-1-1 (Takita et al., 2019)) resulting in the truncation of the last 467 amino acids (Figure 1A, arrow in zebrafish EYS). *lrp5*^{sa11097} carries a nonsense mutation C>A (Figure S1B; Y284X in Lrp5 variant 1, XP_009296098.1, or Lrp5-1; Figure 1A, arrow in zebrafish LRP5). These heterozygous mutants were crossed to generate *eys*$^{+/-}$; *lrp5*$^{+/-}$, *eys*$^{-/-}$, or *lrp5*$^{-/-}$ mutants. The primer pairs used for genotyping are listed in Table S1.

Generation of *rbp1a*$^{-/-}$ zebrafish

The sequence in exon 2 within the lipocalin domain (position 157-179, CAGCTACCTCATCCTAGATAAGG, of NM_001114899.1) was chosen for the target of CRISPR/Cas9-meidiated *rbp1a* gene knockout.

Six μM gRNA was formed by mixing the equimolar of custom-synthesized crRNA and tracrRNA (Integrated DNA technologies (IDT)) with the following parameters: 95°C for 5 min, 85°C for 1 sec, 85-25°C at -2°C/sec, 25°C for 30 sec, 25-16°C at 0.1°C /sec and hold at 16°C. Cas9 protein (Alt-R S.p. HiFi Cas9 Nuclease V3 (IDT) (Vakulskas et al., 2018)) was diluted to 1 μg/μL (~ 6.11 μM) with Injection Buffer and stored at -20°C until use. Same volume of the gRNA and Cas9 protein were then incubated at 37°C for 10 min to form ctRNP prior to injection. ~ 2-3 nL of the ctRNP in 0.15 M KCl solution containing 0.05% phenol red was injected into zebrafish eggs at one-cell stage. The eggs were raised in Raising Medium at 28°C.

At 24 hpf, small pool of the injected embryos was subjected to gene editing. Each embryo was lysed by heating at 95 °C for 30 min in 20 μL of alkaline lysis buffer (25 mM NaOH, 0.25 mM EDTA) (Meeker et al., 2007). Then the solution was neutralized by 1/10th volume of neutralization buffer (1 M Tris-HCl, pH 7.4). The samples were next

subjected to genomic PCR with KOD FX Neo (Toyobo, Osaka, Japan) as follows after being held at 94°C for 2 min: 98°C for 10 sec, then at 55°C for 25 sec and finally at 72°C for 25 sec. The reactions were repeated for 35 cycles. Amplification was checked with 1% agarose gel electrophoresis (Nacalai Tesque, Kyoto, Japan). The primer pair used is listed in Table S1. The PCR product was then subjected to heteroduplex mobility assay (HMA). Heteroduplex DNA was formed using the same parameter that was used in forming the gRNA. Samples were separated on a nondenaturing 10% polyacrylamide gel [10% acrylamide (37.5:1), 1x TBE, 0.1% ammonium persulfate, 0.1% TEMED] and run in 1x TBE buffer. Remaining zebrafish in the pools of embryos were further raised to adulthood and crossed with wildtype to generate F_1. Genomic DNA was extracted from the F_1 zebrafish and genomic PCR was performed with the same primer pair in Table S1. The second round of PCR with the same primer pair was performed by ExTaq (TaKaRa, Kusatsu, Japan) using the PCR product as a template and the subsequent PCR product was purified with NucleoSpin gel and PCR Clean-up (Macherey-Nagel, Düren, Germany). The purified PCR product was cloned into pTAK-2 vector (Biodynamics Laboratory Inc., Tokyo, Japan) and the sequences of mutations in the *rbp1a* gene was analyzed by DNA sequencing with T7 or SP6 primer. An individual that had a deletion of 6 nucleotides (CCTAGA, nucleotide position 169-174 of NM_001114899.1) and an insertion of a

nucleotide (G) in the deleted region (Figure S1C), which leads frameshift after the first 38 amino acids of NP_001108371.1 resulting in the premature stop codon, was chosen for the establishment of the *rbp1a* knockout line.

Generation of *prom1a*$^{-/-}$; *prom1b*$^{-/-}$ zebrafish

The target of the CRISPR/Cas9-meidiated *prom1a* gene knockout was ~~An~~ immediately downstream from the translation start site in the signal peptide sequence region (position 349-371, GTGCTGGGGCTTGACGTCCGGGG, of XM_021480968.1 or transcript variant 1 of *prom1a* (*prom1a-1*)) that all known 13 transcript variants possess in their N-termini of coding sequences. An individual that had a deletion of 13 nucleotides (Figure S1D; nucleotide position 358-370 of *prom1a-1*), which leads frameshift immediately after the start codon (first 13 amino acids of XP_021336643.1), was chosen for the establishment of the *prom1a* knockout line. The primer pair used for the genomic PCR to confirm the mutation and for subsequent genotyping is listed in Table S1.

The *prom1b*^{sa13905} (*prom1b*$^{+/-}$) zebrafish were obtained from the ZIRC. *prom1b*^{sa13905} carries a nonsense mutation G>A (Figure S1E; W15X in Prom1b variant 1 (Prom1b-1; XP_021336908.1)) resulting in the truncation after the first 14 amino acids in the signal peptide sequence region (position 354 of XM_021481233.1 or transcript variant 1 of

prom1b (*prom1b-1*)). All known 8 transcript variants possess the nonsense mutation in their N-termini of coding sequences. The primer pair used for genotyping is listed in Table S1. The *prom1a*$^{-/-}$; *prom1b*$^{-/-}$ zebrafish were generated by crossing *prom1a*$^{+/-}$; *prom1b*$^{+/-}$ mutants.

Genotyping

Caudal fins were lysed by heating at 95 °C for 30 min in 20 μL of alkaline lysis buffer (25 mM NaOH, 0.25 mM EDTA) (Meeker et al., 2007). The solution was neutralized by 1/10th volume of neutralization buffer (1 M Tris-HCl, pH 7.4). The samples were subjected to genomic PCR as follows after held at 94°C for 2 min: 98°C for 10 sec, then at 55°C for 30 sec and finally at 72°C for 30 sec. The reactions were repeated for 35 cycles. Amplification was checked with 1% agarose gel (Nacalai Tesque) and the PCR products were purified with NucleoSpin gel and PCR Clean-up (Macherey-Nagel, Düren, Germany). Direct sequencing was performed with the purified PCR products using BigDye Terminator v3.1 Cycle Sequencing Kit and 3130*xl* Genetic Analyzer (Thermo Fisher Scientific, Waltham, MA, USA).

Observation of the PRCL in the digenic *eys*$^{+/-}$; *lrp5*$^{+/-}$ and wildtype zebrafish eyes

Light-adapted 6 or 14 mpf adult eyes were fixed and embedded in a mixture of OCT compound (Tissue tech) as described (Takita et al., 2016). The adult eyes were cryosectioned at 12 μm thickness. After dried for 1 hr at room temperature, the sections were washed three times with phosphate-buffered saline (PBS; 10 mM Na_2HPO_4, 1.8 mM KH_2PO_4, 140 mM NaCl, 2.7 mM KCl, pH 7.3) containing 0.1% Triton X-100 (PBST) for 5 min. Then the sections were stained with propidium iodide (PI; 1 μg/mL in PBS) for 1h at room temperature in darkness. After the staining, the sections were washed three times with PBS for 5 min and mounted with VECTASHIELD mounting medium (Vector Laboratories).

The zebrafish eyes were imaged with inverted confocal microscope (LSM510 PASCAL, Zeiss) with Fluar 5×/0.25 or Plan-Apochromat 20×/0.8 NA objective lens.

Detection of apoptotic cells

Apoptosis in the mutant adult eyes was examined by TUNEL staining using *In Situ* Cell Death Detection Kit, Fluorescein (Roche) essentially according to the manufacturer's instruction. Briefly, adult eyes at 8 mpf fixed with 4% paraformaldehyde (PFA) in PBS for 8 h were cryosectioned at 12 μm thickness and dried for 1 hr. The sections were washed twice with PBS for 5 min. Then the sections were fixed with 4% PFA in PBS for

20 min. After washed with PBS for 30 min, the samples were permeabilized with 0.1% (w/v) Triton X-100/0.1% sodium citrate for 2 min on ice and washed twice with PBS for 5 min. The sections were incubated with 50 μL of TUNEL reaction mixture in a humidified chamber for 1 hr at 37°C in darkness. The reaction mixture was washed away three times with PBS for 5 min and the sections were embedded with VECTASHIELD (Vector Laboratories) and observed with inverted confocal microscope (LSM510 PASCAL, Zeiss) with EC Plan-Neofluar 10×/0.3 NA objective lens.

Immunohistochemistry

Adult retinas were immunostained basically according to the method described previously (Takita et al., 2016). Rabbit anti-zebrafish Rbp1a and Lrp5 antibodies were raised by GL Biochem (Shanghai, China). Antigen for anti-zebrafish Rbp1a was a synthetic peptide, ^{42}KEIVQNGDHLYIKTLTTFRNYD^{63}, of zebrafish Rbp1a protein (NP_001108371.1). Antigen for anti-zebrafish Lrp5 was a synthetic peptide, ^{1551}DYTTSRWKSNKYYMDLNSDSDP^{1572}, of zebrafish Lrp5 protein (XP_009296098.1). To validate the specificity of the anti-Lrp5 antibody, *lrp5 (Ct)*$^{-/-}$ was generated using CRISPR/Cas9 system and used for the immunohistochemistry. The sequence (Figure S1F; position 4757-4779, CCCCCCACCACCCCCTGCAGCAC, of

XM_009297823.3 or transcript variant 1 of *lrp5* (*lrp5-1*)) immediately upstream of the sequence encoding the antigen was chosen as the target to minimize any potential reactions that might hinder the proper validation: other potential minor wildtype *lrp5* transcript variant(s) and/or cryptic splicing that could escape the intended knockout of the gene as a result of the knockout.

The antibodies were purified with Protein A HP SpinTrap (Cytiva, Madison, Wisconsin, USA) and used for immunohistochemistry (anti-Rbp1a antibody, 1:75000 dilution; anti-Lrp5 antibody, 1:500000 dilution). For double staining of antibodies raised in the same species, the antibodies were labeled with Ab-10 Rapid HiLyte Fluor^{TM} 555 Labeling Kit (Dojindo Molecular Technologies, Inc.) prior to use. Microvilli of RPE cells were visualized with rabbit anti-MOESIN (MSN) antibody (Proteintech, 16495-1-AP; 1:1000 dilution). The processes of Müller cells were visualized with rabbit anti-GFAP (Agelent (Dako), Z0334; 1:4000 dilution) and mouse anti-GS (Merck, MAB302 (clone GS-6); 1:1000 dilution) antibodies. Alexa Fluor 488 goat anti-rabbit antibody (1:500 or 1:1000 dilution) was purchased from Thermo Fisher Scientific.

The sections were embedded with VECTASHIELD (Vector Laboratories) and observed with inverted confocal microscope (LSM510 PASCAL, Zeiss) with EC Plan-Neofluar 40×/1.3 NA objective lens. Z-stack images (captured with a 0.45 μm step size)

were acquired, maximum intensity projection (MIP) was generated from the Z-stack images with ZEN 2011 Black Edition (Zeiss), and generated images were checked manually. Representative MIP images were selected for image presentation.

Microarray analysis

Total RNA was isolated from light-adapted 3.5 mpf adult three zebrafish as described (Takita et al., 2016). Briefly, zebrafish were sacrificed in the ice-cold fresh-water three hours after light onset. Eyes were then detached and the water and blood that remained were quickly wiped away as much as possible. The eyes were homogenized with 200 μL of TRI Reagent (Merck) and total RNA was isolated according to the manufacture's instructions. The concentration was quantified spectrophotometrically and microarray was performed with 250 ng of the total RNA on Genechip Zebrafish Gene 1.0 ST Array (Thermo Fisher Scientific). Acquired data were analyzed by Transcriptome Analysis Console (TAC) 4.0.1 (Thermo Fisher Scientific).

qPCR

First-strand cDNA was synthesized from 1 μg of the saved total RNA used for microarray by reverse transcription at 50°C for 2 hr using SuperScript IV reverse

transcriptase (Thermo Fisher Scientific, Waltham, MA, USA) primed with the supplied random primer and cDNAs were stored at -25°C until use. Isolation of total RNA and cDNA synthesis for other mutants were performed similarly. To measure the expression levels of *rbp1a*, *rbp1b*, *lrp5*, *prom1a*, *prom1b*, or *eys* mRNA, the average expression level of each mRNA was obtained from three samples (n = 3) with Platinum™ SYBR™ Green qPCR SuperMix-UDG (Thermo Fisher Scientific). The primer pairs used are listed in Table S2.

Binding assay

Full-length *rbp1a* and C-terminal intracellular region of *lrp5* were amplified from zebrafish eye cDNA by RT-PCR using the primer pairs listed in Table S3, cloned into pTAK-2 vector (BioDynamics Laboratory Inc.), and sequenced. The *rbp1a* fragment was fused with EGFP-HAT and subcloned into pTAK-2 vector. After the sequence was verified, the insert was excised with EcoRI and SalI and ligated to the corresponding site of pGEX-5X-1 (Cytiva) to obtain an N-terminally GST-fused and C-terminally EGFP-HAT-fused product (pGEX-5x-1-Drerbp1a-EGFP encoding GST-Rbp1a-EGFP).

The *lrp5* fragment was fused with mCherry and subcloned into pTAK-2 vector. After the sequence was verified, the insert was excised with EcoRI and SalI and ligated to the

corresponding site of pMAL-c2E (New England Biolabs) to obtain an N-terminally MBP-fused and C-terminally mCherry-fused product (pMAL-c2E-Drelrp5(C-terminal)-mCherry encoding MBP-Lrp5(intracellular)-mCherry). pMAL-c2E for MBP expression was previously described (Takita et al., 2016).

Each plasmid was transformed into *E. coli* BL21 (DE3) for expression. A suspension of *E. coli* expressing the GST-Rbp1a-EGFP, MBP, or MBP-Lrp5(intracellular)-mCherry protein was sonicated and the supernatant was collected. The supernatant was loaded to Glutathione Sepharose-4B (Cytiva) or amylose beads (New England Biolabs) and GST-Rbp1a-EGFP was further purified according to the manufacturer's instruction. Purified GST-Rbp1a-EGFP and MBP- or MBP-Lrp5(intracellular)-mCherry-bound amylose beads were kept at 4°C until use.

The purified GST-Rbp1a-EGFP (20 μL) was incubated in 200 μL of PBS containing 5 μL of the amylose beads pre-bound with either MBP or MBP-Lrp5(intracellular)-mCherry for 24 h at 4°C. Then the beads were centrifuged at 2000 *g* for 2 min at 4°C. The precipitated beads were washed three times with 200 μL of PBS and mounted on a slide with VECTASHIELD (Vector Laboratories) for observation. Fluorescence on the beads was observed under an inverted confocal microscope (LSM 510 PASCAL, Zeiss) with Plan-Apochromat 20×/0.8 NA objective lens.

Image analysis

The thickness of PRCL in wildtype or the mutant eyes was measured based on the previous study (Lu et al., 2017). Briefly, the region 100 μm away from the optic nerve head was chosen and the thickness of PRCL was measured with ZEN 2011 Black Edition (Zeiss). The thickness of *eys*$^{+/-}$; *lrp5*$^{+/-}$ mutant PRCL was compared with age-matched wildtype. Three zebrafish from each group were used. The number of nuclei in the ONL in wildtype or the mutant eyes was counted manually using the same image acquired for the measurement of the thickness of PRCL.

Fluorescence on the surface of the beads in Figure 4F was analyzed with ImageJ (Rasband, W.S., ImageJ, National Institutes of Health, Bethesda, MD). The images were converted to 8-bit representations. The beads then were enclosed manually with oval selection and the mean for the area was measured. Background signal determined from the area where there were no bead was subtracted from the mean. The resulting value was assigned as the fluorescence for a single bead.

Acquired images shown in Figure S4 were analyzed with ImageJ. After signal intensity of each pixel in the image was converted to an 8-bit representation, plot profiles were generated with the line plot from the left red arrowhead to the right red arrowhead.

Statistical analysis

For the measurements of the thickness of PRCL and number of nuclei in the ONL in wildtype or mutant zebrafish and the expression levels of *rbp1a*, *rbp1b*, *lrp5*, *prom1a*, *prom1b*, or *eys* mRNA, data are presented as mean ± standard deviation (SD), and levels of significance (*P* value, Student's t-test) are indicated in the figure legends.

Supplemental References

Kettleborough, R.N., Busch-Nentwich, E.M., Harvey, S.A., Dooley, C.M., de Bruijn, E., van Eeden, F., Sealy, I., White, R.J., Herd, C., Nijman, I.J.*, et al.* (2013). A systematic genome-wide analysis of zebrafish protein-coding gene function. Nature 496, 494-497.

Lu, Z., Hu, X., Liu, F., Soares, D.C., Liu, X., Yu, S., Gao, M., Han, S., Qin, Y., Li, C.*, et al.* (2017). Ablation of EYS in zebrafish causes mislocalisation of outer segment proteins, F-actin disruption and cone-rod dystrophy. Sci Rep 7, 46098.

Meeker, N.D., Hutchinson, S.A., Ho, L., and Trede, N.S. (2007). Method for isolation of PCR-ready genomic DNA from zebrafish tissues. Biotechniques 43, 610, 612, 614.

Takita, S., Miyamoto-Matsui, K., and Seko, Y. (2019). Intra- and interspecies comparison of EYS transcripts highlights its characteristics in the eye. FASEB J 33, 9422-9433.

Takita, S., Wada, Y., and Kawamura, S. (2016). Effects of NDRG1 family proteins on photoreceptor outer segment morphology in zebrafish. Sci Rep 6, 36590.

Vakulskas, C.A., Dever, D.P., Rettig, G.R., Turk, R., Jacobi, A.M., Collingwood, M.A., Bode, N.M., McNeill, M.S., Yan, S., Camarena, J.*, et al.* (2018). A high-fidelity Cas9 mutant delivered as a ribonucleoprotein complex enables efficient gene editing in human hematopoietic stem and progenitor cells. Nat Med 24, 1216-1224.